SUPPLEMENTAL INFORMATION

Intrinsically disordered protein regions are required for cell wall homeostasis in *Bacillus subtilis*

Yannick R. Brunet, Cameron Habib, Anna P. Brogan, Lior Artzi, and David Z. Rudner

This PDF file includes:

SUPPLEMENTAL METHODS

Strain and plasmid construction

Deletion strains

Insertion-deletion mutants were from the *Bacillus* knock-out (BKE) collection (Koo et al. 2017) or were generated by isothermal assembly (Gibson 2011) of PCR products followed by direct transformation into *B*. *subtilis*. All BKE mutants were back-crossed twice into *B*. *subtilis* PY79. All deletions were confirmed by PCR. Antibiotic cassette removal was performed using a temperature-sensitive plasmid that constitutively expresses Cre recombinase (Meeske et al. 2015).

The following oligonucleotide primers were used to make the indicated strains: *(sigI-rsgI)::spec* (oYB213/214, oYB180/181); *ecsAB::spec* (oYB205/206, oYB207/208); (*sigM-yhdL-yhdK)::erm* (oIR40/24, oIR25/43); *rasP::tet* (oYB201/202, oYB203/204); *gpsB::tet* and *gpsB::spec* (oIR431/432, oIR433,434), *rsgI::kan* and *rsgI::spec* (oYB178/179, oYB180/181); *ponA::kan* (oYB402/403, oYB404/405); *ecsA::erm* (BKE collection); *ecsB::erm* (BKE collection); *rasP::erm* (BKE collection); *sigI::erm* (BKE collection). Antibiotic cassettes were amplified with oWX438/439 or oJM28/oJM29 for Δ*(sigM-yhdL-yhdK)::erm, gpsB::tet* and *gpsB::spec*.

Plasmid construction

pAM13: *ycgO::Pspank-ponA (cat)* was generated by ligation with a XmaI-SpeI PCR product encoding the *ponA* (amplified with oligonucleotide primers oAM62 and oAM64 from PY79 genomic DNA) and pAM11 [*ycgO::Pspank (cat)*].

pAM14: *ycgO::Pspank*-ponA (cat)* was generated by ligation with a XmaI-SpeI PCR product encoding the *ponA* (amplified with oligonucleotide primers oAM62 and oAM64 from PY79 genomic DNA) and pAM12 [*ycgO::Pspank* (cat)*].

pLA98: *ycgO::Pspank-ponAΔID (cat)* was generated in a 2-way isothermal assembly reaction (Gibson 2011) with a PCR product containing *ponA-ΔID* (amplified with oligonucleotide primers oLA196 and oYB191 from PY79 genomic DNA) and pAM11 [*ycgO::Pspank (cat)*] cut with XmaI and SpeI.

pYB72: *amyE::sigI-rsgI-S481 (kan)* was generated in a 2-way isothermal assembly reaction with a PCR product containing *sigI-rsgI-S481* (amplified with oligonucleotide primers oYB197 and oYB217 from PY79 genomic DNA) and pER82 [*amyE::kan*] cut with BamHI and EcoRI. *S481* is the 3' untranslated region in the *sigI-rsgI* transcript.

pYB110: ***yvbJ::PxylA-gfp-rsgI (erm)*** was generated in a 2-way isothermal assembly reaction with a PCR product containing *rsgI* (amplified with oligonucleotide primers oYB294 and oYB295 from PY79 genomic DNA) and pRB77 [*yvbJ::PxylA-gfp (erm)*] cut with BamHI and XhoI.

pYB117: ***yvbJ::PxylA-gfp-rsgI-His (erm)*** was generated in a 2-way isothermal assembly reaction with a PCR product containing *rsgI-His* (amplified with oligonucleotide primers oYB294 and oYB304 from PY79 genomic DNA) and pRB77 [*yvbJ::PxylA-gfp (erm)*] cut with BamHI and XhoI.

pYB119: ***yvbJ::PxylA-gfp-rsgI(D95A) (erm)*** was generated in a 3-way isothermal assembly reaction with two PCR products containing *rsgI-D95A' and 'rsgI-D95A* (amplified with oligonucleotide primers oYB294/249 and oYB250/295 from PY79 genomic DNA) and pRB77 [*yvbJ::PxylA-gfp (erm)*] cut with BamHI and XhoI.

pYB120: ***yvbJ::PxylA-gfp-rsgI(D95N) (erm)*** was generated in a 3-way isothermal assembly reaction with two PCR products containing *rsgI-D95N' and 'rsgI-D95N* (amplified with oligonucleotide primers oYB294/251 and oYB252/295 from PY79 genomic DNA) and pRB77 [*yvbJ::PxylA-gfp (erm)*] cut with BamHI and XhoI.

pYB121: ***yvbJ::PxylA-gfp-rsgI(N97A) (erm)*** was generated in a 3-way isothermal assembly reaction with two PCR products containing *rsgI-N97A' and 'rsgI-N97A* (amplified with oligonucleotide primers oYB294/253 and oYB254/295 from PY79 genomic DNA) and pRB77 [*yvbJ::PxylA-gfp (erm)*] cut with BamHI and XhoI.

pYB122: ***yvbJ::PxylA-gfp-rsgI(N117A) (erm)*** was generated in a 3-way isothermal assembly reaction with two PCR products containing *rsgI-N117A' and 'rsgI-N117A* (amplified with oligonucleotide primers oYB294/255 and oYB256/295 from PY79 genomic DNA) and pRB77 [*yvbJ::PxylA-gfp (erm)*] cut with BamHI and XhoI.

pYB138: ***yvbJ::PxylA-gfp-rsgI(D95A)-His (erm)*** was generated in a 3-way isothermal assembly reaction with two PCR products containing *rsgI-D95A-His' and 'rsgI-D95A-His* (amplified with oligonucleotide primers oYB294/249 and oYB250/304 from PY79 genomic DNA) and pRB77 [*yvbJ::PxylA-gfp (erm)*] cut with BamHI and XhoI.

pYB182: ***ycgO::PbcrC-optRBS-lacZ (erm)*** was generated in a 2-way isothermal assembly reaction with a PCR product containing *PbcrC* (amplified with oligonucleotide primers oYB386 and oYB387 from PY79 genomic DNA) and pYB64 [*ycgO::Pveg-lacZ (Opt RBS) (erm)*] cut with HindIII and EcoRI.

pYB193: ***amyE::PbcrC-optRBS-lacZ (cat)*** was generated by ligation with a HindIII-BamHI *lacZ* insert from pYB64 [*ycgO::Pveg-optRBS-lacZ (erm)*] and pYB181 [*amyE::PbcrC-optRBS-venus (cat)*] cut with HindIII and BamHI.

pYB196: ***amyE::sigI-rsgIΔID-ID(RsgI-Bc14579)-S481 (kan)*** was generated in a 4-way isothermal assembly reaction with three PCR products containing *sigI-rsgIΔID*, *ID(rsgi-Bc14)* and *S481* (amplified with oligonucleotide primers oYB197 and oYB411, oYB408 and oYB409 and oYB410 and oYB217 from PY79 genomic DNA and *B. cereus* 14579 genomic DNA) and pER82 [amyE::kan] cut with BamHI and EcoRI.

pYB200: ***yvbJ::PxylA-gfp-His (erm)*** was generated in a 2-way isothermal assembly reaction with a PCR product containing *hisx6* (amplified with oligonucleotide primers oYB420 and oYB421 from PY79 genomic DNA) and pRB77 [*yvbJ::PxylA-gfp (erm)*] cut with BamHI and XhoI.

pYB201: ***yhdG::PbcrC-optRBS-lacZ (cat)*** was generated in a 2-way isothermal assembly reaction with a PCR product containing *Pbcr-lacZ* with an optimized *RBS* (amplified with oligonucleotide primers oYB422 and oYB423 from pYB182) and pCB08 [*yhdG::cat*] cut with BamHI and EcoRI.

pYB202: ***amyE::sigI-rsgIΔID-NheI-S481 (kan)*** was generated in a 3-way isothermal assembly reaction with two PCR products containing *sigI-rsgIΔID* and *S481* (amplified with oligonucleotide primers oYB197 and oYB425, and oYB217 and oYB424 from PY79 genomic DNA) and pER82 [*amyE::kan*] cut with BamHI and EcoRI.

pYB207: ***amyE::sigI-rsgIΔID-ID(PBP1-Bc14579)-S481 (kan)*** was generated in a 2-way isothermal assembly reaction with a PCR product containing *ID(ponA-Bc14579)* (amplified with oligonucleotide primers oYB433 and oYB434 from *B. cereus* 14579 genomic DNA) and pYB202 [amyE::sigI-rsgIΔID-NheI-S481 (kan)] cut with NheI.

pYB208: ***amyE::sigI-rsgIΔID-ID(PBP1-BcB4088)-S481 (kan)*** was generated in a 2-way isothermal assembly reaction with a PCR product containing *ID(PBP1-BcB4088)* (amplified with oligonucleotide primers oYB435 and oYB436 from a *ID(ponA B. cereus B4088)* gBlock (IDT)) and pYB202 [amyE::sigI-rsgIΔID-NheI-S481 (kan)] cut with NheI.

pYB209: ***amyE::sigI-rsgIΔID-ID(PBP1-BcJRS1)-S481 (kan)*** was generated in a 2-way isothermal assembly reaction with a PCR product containing *ID(ponA-BcJRS1)* (amplified with oligonucleotide primers oYB437 and oYB438 from a *ID(PBP1 B. cereus JRS1)* gBlock (IDT)) and pYB202 [amyE::sigI-rsgIΔID-NheI-S481 (kan)] cut with NheI.

pYB210: ***amyE::sigI-rsgIΔID-SpoIVFA(ECD)-S481 (kan)*** was generated in a 2-way isothermal assembly reaction with a PCR product containing *spoIVFA(ECD)* (amplified with oligonucleotide primers oYB439 and oYB440 from PY79 genomic DNA) and pYB202 [amyE::sigI-rsgIΔID-NheI-S481 (kan)] cut with NheI.

pYB212: ***ycgO::Pspank-ponA-ΔID-ID(RsgI Bs) (cat)*** was generated in a 2-way isothermal assembly reaction with a PCR product containing *ID(RsgI Bs)* (amplified with oligonucleotide primers oYB443 and oYB444 from PY79 genomic DNA) and pLA98 [*ycgO::Pspank-ponA-ΔID (cat)*] cut with SpeI.

pYB213: ***ycgO::Pspank-ponA-ΔID-ID(RsgI Bc14579) (cat)*** was generated in a 2-way isothermal assembly reaction with a PCR product containing *ID(RsgI Bc14579)* (amplified with oligonucleotide primers oYB445 and oYB446 from *B. cereus* 14579 genomic DNA) and pLA98 [*ycgO::Pspank-ponA-ΔID (cat)*] cut with SpeI.

pYB214: ***ycgO::Pspank-ponA-ΔID-ID(PBP1 Bc14579) (cat)*** was generated in a 2-way isothermal assembly reaction with a PCR product containing *ID(PBP1 Bc14579)* (amplified with oligonucleotide primers oYB447 and oYB448 from *B. cereus* 14579 genomic DNA) and pLA98 [*ycgO::Pspank-ponA-ΔID (cat)*] cut with SpeI.

pYB215: ***ycgO::Pspank-ponA-ΔID-ID(PBP1 BcB4088) (cat)*** was generated in a 2-way isothermal assembly reaction with a PCR product containing *ID(PBP1 BcB4088)* (amplified with oligonucleotide primers oYB449 and oYB450 from a *ID(PBP1 B. cereus B4088)* gBlock (IDT)) and pLA98 [*ycgO::Pspank-ponA-ΔID (cat)*] cut with SpeI.

pYB216: ***ycgO::Pspank-ponA-ΔID-ID(PBP1 BcBJRS1) (cat)*** was generated in a 2-way isothermal assembly reaction with a PCR product containing *ID(PBP1 BcBJRS1)* (amplified with oligonucleotide primers oYB451 and oYB452 from a *ID(PBP1 B. cereus BcBJRS1)* gBlock (IDT)) and pLA98 [*ycgO::Pspank-ponA-ΔID (cat)*] cut with SpeI.

pYB217: ***ycgO::Pspank-ponA-ΔID-SpoIVFA (ECD) (cat)*** was generated in a 2-way isothermal assembly reaction with a PCR product containing *spoIVFA-ECD* (amplified with oligonucleotide primers oYB453 and oYB454 from PY79 genomic DNA) and pLA98 [*ycgO::Pspank-ponA-ΔID (cat)*] cut with SpeI.

pYB222: ***amyE::sigI-rsgIΔID-ID(Pl)-S481 (kan)*** was generated in a 2-way isothermal assembly reaction with a PCR product containing *ID(Pl)* (amplified with oligonucleotide primers oYB464 and oYB465 from a *ID(P. luteus)* gBlock (IDT)) and pYB202 [amyE::sigI-rsgIΔID-NheI-S481 (kan)] cut with NheI.

pYB223: ***amyE::sigI-rsgIΔID-ID(Bp)-S481 (kan)*** was generated in a 2-way isothermal assembly reaction with a PCR product containing *ID(Bp)* (amplified with oligonucleotide primers oYB466 and oYB467 from a *ID(B. pumilus)* gBlock (IDT)) and pYB202 [amyE::sigI-rsgIΔID-NheI-S481 (kan)] cut with NheI.

pYB225: ***amyE::sigI-Nhe1-S481 (kan)*** was generated in a 3-way isothermal assembly reaction with two PCR products containing *sigI-nhe1* and *nhe1-S481* (amplified with oligonucleotide primers oYB197/469 and oYB470/217 from PY79 genomic DNA) and pER82 [*amyE::kan*] cut with BamHI and EcoRI.

pYB226: ***amyE::sigI-rsgI(Y91S)-S481 (kan)*** was generated in a 2-way isothermal assembly reaction with two PCR products containing *rsgI(Y91S)'* and *'rsgI(Y91S)* (amplified with oligonucleotide primers oYB471/473 and oYB472/474 from PY79 genomic DNA) and pYB225 [*amyE::sigI-Nhe1-S481-UTR (kan)*] cut with NheI.

pYB228: ***amyE::sigI-rsgI(E101A)-S481 (kan)*** was generated in a 2-way isothermal assembly reaction with two PCR products containing *rsgI(E101A)'* and *'rsgI(E101A)* (amplified with oligonucleotide primers oYB471/478 and oYB472/477 from PY79 genomic DNA) and pYB225 [*amyE::sigI-Nhe1-S481-UTR (kan)*] cut with NheI.

pYB229: ***amyE::sigI-rsgI(E119A)-S481 (kan)*** was generated in a 2-way isothermal assembly reaction with two PCR products containing *rsgI(E119A)'* and *'rsgI(E119A)* (amplified with oligonucleotide primers

oYB471/480 and oYB472/479 from PY79 genomic DNA) and pYB225 [*amyE::sigI-Nhe1-S481-UTR (kan)*] cut with NheI.

pYB231: ***amyE::sigI-rsgI(V110A)-S481 (kan)*** was generated in a 2-way isothermal assembly reaction with two PCR products containing *rsgI(V110A)'* and *'rsgI(V110A)* (amplified with oligonucleotide primers oYB471/484 and oYB472/483 from PY79 genomic DNA) and pYB225 [*amyE::sigI-Nhe1-S481-UTR (kan)*] cut with NheI.

pYB232: ***amyE::sigI-rsgI(P98A)-S481 (kan)*** was generated in a 2-way isothermal assembly reaction with two PCR products containing *rsgI(P98A)'* and *'rsgI(P98A)* (amplified with oligonucleotide primers oYB471/486 and oYB472/485 from PY79 genomic DNA) and pYB225 [*amyE::sigI-Nhe1-S481-UTR (kan)*] cut with NheI.

pYB228: ***amyE::sigI-rsgI(E101A)-S481 (kan)*** was generated in a 2-way isothermal assembly reaction with two PCR products containing *rsgI(P98A)'* and *'rsgI(P98A)* (amplified with oligonucleotide primers oYB471/478 and oYB472/477 from PY79 genomic DNA) and pYB225 [*amyE::sigI-Nhe1-S481-UTR (kan)*] cut with NheI.

pYB246b: ***amyE::sigI-rsgI(D95A)-S481 (kan)*** was generated in a 2-way isothermal assembly reaction with two PCR products containing *rsgI(P98A)'* and *'rsgI(P98A)* (amplified with oligonucleotide primers oYB471/249 and oYB472/250 from PY79 genomic DNA) and pYB225 [*amyE::sigI-Nhe1-S481-UTR (kan)*] cut with NheI.

pYB240: ***yvbJ::PxylA-gfp-rsgIΔID-His (erm)*** was generated in a 2-way isothermal assembly reaction with a PCR product containing *rsgI-ΔID* (amplified with oligonucleotide primers oYB294 and oYB507 from PY79 genomic DNA) and pYB200 [*yvbJ::PxylA-gfp-His (erm)*] cut with BamHI.

pYB241: ***yvbJ::PxylA-gfp-rsgIΔID-ID(RsgI Bc14579)-His (erm)*** was generated in a 2-way isothermal assembly reaction with a PCR product containing *rsgI-ΔID-ID(RsgI Bc14)* (amplified with oligonucleotide primers oYB294 and oYB508 from pYB196 [amyE::sigI-rsgIΔID-ID(RsgI-Bc14)-S481 (kan)]) and pYB200 [*yvbJ::PxylA-gfp-His (erm)*] cut with BamHI.

pYB243: ***yvbJ::PxylA-gfp-rsgIΔID-ECD(spoIVFA)-His (erm)*** was generated in a 2-way isothermal assembly reaction with a PCR product containing *rsgI-ΔID-SpoIVFA (ECD)* (amplified with oligonucleotide primers oYB294 and oYB510 from pYB210 [amyE::sigI-rsgIΔID-*SpoIVFA (ECD)*-S481 (kan)]) and pYB200 [*yvbJ::PxylA-gfp-His (erm)*] cut with BamHI.

pYB246: ***amyE::sigI-rsgI(D95A)-S481 (kan)*** was generated in a 2-way isothermal assembly reaction with two PCR products containing *rsgI(D95A)'* and *'rsgI(D95A)* (amplified with oligonucleotide primers oYB471/249 and oYB472/250 from PY79 genomic DNA) and pYB225 [*amyE::sigI-Nhe1-S481-UTR (kan)*] cut with NheI.

pYB252: ***yvbJ::PxylA-gfp-rsgIΔID-ID(PBP1 BcB4088)-His (erm)*** was generated in a 2-way isothermal assembly reaction with a PCR product containing *rsgI-ΔID-ID(PBP1 BcB4088)* (amplified with oligonucleotide primers oYB294 and oYB519 from pYB208 [amyE::sigI-*rsgI-ΔID-ID(PBP1 BcB4088)*-S481 (kan)]) and pYB200 [*yvbJ::PxylA-gfp-His (erm)*] cut with BamHI.

pYB254: ***amyE::sigI-rsgIΔID-ID(Bs-scramble1)-S481 (kan)*** was generated in a 2-way isothermal assembly reaction with a PCR product containing *ID(Bs-scramble #1)* (amplified with oligonucleotide primers oYB528 and oYB529 from a *ID(B. subtilis scramble #1)* gBlock (IDT)) and pYB202 [amyE::sigI-rsgIΔID-NheI-S481 (kan)] cut with NheI.

pYB255: ***amyE::sigI-rsgIΔID-ID(Bs-scramble2)-S481 (kan)*** was generated in a 2-way isothermal assembly reaction with a PCR product containing *ID(Bs-scramble #2)* (amplified with oligonucleotide primers oYB530 and oYB531 from a *ID(B. subtilis scramble #2)* gBlock (IDT)) and pYB202 [amyE::sigI-rsgIΔID-NheI-S481 (kan)] cut with NheI.

pYB259: ***His-sumo-ponA (amp)*** was generated in a 2-way isothermal assembly reaction with a PCR product containing *ponA* (amplified with oligonucleotide primers oYB544 and oYB545 from PY79 genomic DNA) and pTD68 [*His-sumo* (amp)] cut with BamHI/XhoI.

pYB260: ***His-sumo-ponAΔID (amp)*** was generated in a 2-way isothermal assembly reaction with a PCR product containing *ponA* (amplified with oligonucleotide primers oYB544 and oYB546 from PY79 genomic DNA) and pTD68 [*His-sumo* (amp)] cut with BamHI/XhoI.

pCH37: *His-sumo-ponA(E115A) (amp)* was generated in a 2-way isothermal assembly reaction with a PCR product containing *ponA(E115A)* (amplified with oligonucleotide primers oYB544 and oYB545 from bAM0266 gDNA) and pTD68 [*His-sumo* (amp)] cut with BamHI/XhoI.

pYB269: *ycgO::Pspank-ponAΔID-ID(Bs-scramble1) (cat)* was generated in a 2-way isothermal assembly reaction with a PCR product containing *ID(PBP1 Bs scramble #1)* (amplified with oligonucleotide primers oYB559 and oYB560 from a *ID(PBP1 Bs scramble #1)* gBlock (IDT))and pLA98 [*ycgO::Pspank-ponA-ΔID (cat)*] cut with SpeI.

pYB270: *ycgO::Pspank-ponAΔID-ID(Bs-scramble2) (cat)* was generated in a 2-way isothermal assembly reaction with a PCR product containing *ID(PBP1 Bs scramble #2)* (amplified with oligonucleotide primers oYB561 and oYB562 from a *ID(PBP1 Bs scramble #2)* gBlock (IDT))and pLA98 [*ycgO::Pspank-ponA-ΔID (cat)*] cut with SpeI.

All plasmids were sequenced confirmed by Sanger sequencing.

SUPPLEMENTAL FIGURE LEGENDS

Figure S1. Transposon-sequencing identifies *rasP*, *ecsA,* and *ecsB* as synthetic lethal with *cwlO*.
Transposon insertion profiles from wild-type (WT) and Δ*cwlO* libraries. Four regions of the genome are shown. Each vertical line indicates a transposon insertion site; the height reflects the number of sequencing reads at this position. Transposon insertions in *lytE*, *sigI*, *rasP*, *ecsA* and *ecsB* were under-represented in the Δ*cwlO* Tn library compared to wild-type. Maximum reads were normalized to 150 for regions containing *lytE, cwlO*, and *ecsAB*, and 50 for the region with *rasP*.

Figure S2. *rasP*, *ecsA* and *ecsB* are synthetic lethal with *cwlO.*
(A) Validation of the Tn-seq data using an IPTG-regulated allele of *cwlO*. **(B)** Synthetic lethality can be suppressed by Δ*rsgI*. Spot-dilutions of the indicated strains in the presence and absence of 500 μM IPTG. All strains were grown in the presence of inducer to OD600 ~2.0. The cultures were washed without inducer, resuspended to an OD600 of 1.5, and 10-fold serially diluted. Five microliters of each dilution were spotted onto LB agar plates with and without IPTG. The plates for photographed after overnight incubation at 37 ˚C. The synthetic lethality between *sigI* and *rasP*, *ecsA*, and *ecsB* can be suppressed by Δ*rsgI*, placing these genes upstream of the anti-sigma factor.

Figure S3. The σ^{I}-responsive *bcrC* promoter-fusion to *lacZ* is specific to σ^{I}.

(A) Schematic diagram of the *bcrC* promoter region and the σ^{I}-responsive promoter fusion used in this study. **(B)** Bar graph showing β-galactosidase activity from the P(bcrC)-*lacZ* reporter in the indicated strains. The Δ*walH* mutation results in high WalR activity. Activity was assayed in exponentially growing cultures in LB. Error bars represent standard deviation from three biological replicates.

Figure S4. Transposon-sequencing identifies *ponA* and *sigI* as a synthetic lethal pair.

(A-B) Transposon insertion profiles from transposon libraries generated in wild-type (WT) and in the Δ*sigI* mutant. Four genomic regions are shown. The height of each line reflects the number of sequencing reads that map to this position. Tn insertions in *cwlO*, *ftsEX*, *sweDC* and *ponA* are underrepresented in the Δ*sigI* Tn library compared to wild-type. **(C)** Transposon insertion profiles from Tn libraries generated in wild-type (WT) and in a Δ*ponA* P(IPTG)-*ponA* mutant (Δ*ponA*) in the absence of IPTG. Tn insertions in *sigI* are underrepresented in the Δ*ponA* library compared to wild-type. (**D**) σ^{I} activity is increased in the Δ*ponA* mutant. Bar graph showing β-galactosidase activity from the σ^{I}-responsive P(bcrC)-*lacZ* reporter in the indicated strains. Activity was assayed in exponentially growing cultures in LB. Error bars represent standard deviation from three biological replicates. (**E**) Validation of Tn-seq results. Spot dilutions of the indicated strains in the presence and absence of inducer (IPTG).

Figure S5. Functionality of the GFP-RsgI-His fusion.

Bar graph showing β-galactosidase activity from the σ^{I}-responsive P(bcrC)-*lacZ* reporter in the presence (+) and absence (Δ) of *ponA* in the Δ*rsgI* mutant complemented by a xylose-inducible *gfp-rsgI-his* allele. Activity was assayed in exponentially growing cultures in LB supplemented with the indicated concentrations of xylose (in mM). Error bars represent standard deviation from three biological replicates.

Figure S6. Intramembrane cleavage of RsgI in response to PBP1 depletion requires RasP. Representative immunoblots showing the stability of GFP-RsgI-His cleavage products in the indicated strains that lack the native *rsgI* gene and harbor a xylose-regulated allele of *gfp-rsgI-his*. Cells were grown in LB medium supplemented with 20 mM xylose and 50 μM IPTG. The cells were then washed to remove IPTG and grown for 1.5 hours in LB medium with 20 mM xylose to deplete PBP1. At mid-exponential phase they were treated with spectinomycin and chloramphenicol to inhibit protein synthesis. Samples were collected at the indicated time points (in min) before and after addition of antibiotics and GFP-RsgI-His was assessed by immunoblot using anti-His and anti-GFP antibodies. Upon depletion of PBP1, the membrane-anchored site-1 cleavage product was stable over the time course, indicating that further

processing requires RasP. By contrast the extracytoplasmic site-1 cleavage product was unstable, presumably due to release into the culture supernatant.

Figure S7. Multiple sequence alignment of RsgI homologs displayed as a WebLogo. Intracellular domain, transmembrane (TM) segment, extracellular domain, and the poorly conserved disordered region are shown in different shades of purple. Schematic representation of RsgI bound to σ^I (I) is shown on the right.

Figure S8. Alignment of RsgI homologs highlights similarities and differences in the unstructured region. Amino acid alignment of of RsgI homologs from the Bacillaceae family. Amino acid sequences were aligned using Clustal Omega (Madeira et al. 2019) and displayed using T-coffee (Di Tommaso et al. 2011). Conserved residues in the cytoplasmic domain, transmembrane (TM) segment, and the extracytoplasmic juxta-membrane domain are shown in greyscale. The ten most common residues (D/E, K/R, Q/N, S/T, G, P) in the C-terminal unstructured regions are highlighted. Residues with similar properties are colored the same. The boxed region is enlarged below to highlight the similarities and differences among the unstructured regions. The NCBI reference sequence for each RsgI homolog can be found in Table S4.

Figure S9. The C-terminal region of RsgI is predicted to be intrinsically disordered.
Graphical outputs from the indicated prediction programs of intrinsic disorder (Ishida and Kinoshita 2007; Jones and Cozzetto 2015; Madeira et al. 2019; Erdos et al. 2021). All three programs predict that the C-terminal ~160 residues of RsgI are intrinsically disordered.

Figure S10. The juxta-membrane domain of RsgI is required for regulated proteolysis.
(A) Multiple sequence alignment using WebLogo of the TM segment and part of the juxta-membrane domain of RsgI. Below the alignment are predicted secondary structure elements. Amino acid substitutions tested are highlighted above the alignment. Those in red were constitutively cleaved and phenocopied a Δ*rsgI* mutant. **(B)** Immunoblot analysis of GFP-RsgI in the indicated RsgI mutants in the presence and absence of *rasP*. **(C)** Spot dilutions of the indicated mutants harboring the σ^I-responsive P(bcrC)-*lacZ* reporter on LB agar supplemented with X-gal. The strains used in panel C contained *rsgI* that lack GFP- and His-tags.

Figure S11. Site-1-cleaved RsgI products remain associated.
Silver-stained gel of elutions from anti-His immunoprecipitation of GFP-RsgI-His from detergent-solubilized membrane fractions of *B. subtilis* cells expressing GFP-RsgI-His or GFP-RsgI. Black carets highlight the N- and C-terminal site-1 cleavage products identified by mass spectrometry. Molecular weight markers (in kDa) are shown.

Figure S12. Intrinsically disordered regions from *B. cereus* RsgI homologs function in place of the IDR on *B. subtilis* RsgI. Representative immunoblots showing the stability of GFP-RsgI-His cleavage products in the indicated strains. All strains lack the native *rsgI* gene and harbor the indicated variants under xylose-inducible control. Cells were grown in LB medium supplemented with 10 mM xylose to mid-exponential phase and then treated with spectinomycin and chloramphenicol to inhibit protein synthesis. Samples were collected at the indicated time points (in min) before and after addition of antibiotics and GFP-RsgI-His variants were analyzed by immunoblot using anti-His and anti-GFP antibodies.

Figure S13. The chromosomal insertion site of the P(bcrC)-*lacZ* reporter influences the magnitude of the response. Bar graph showing β-galactosidase activity from the σ^I-responsive reporter P(bcrC)-*lacZ* integrated at three chromosomal locations (*amyE*, *ycgO*, and *yhdG*). The location in degrees relative to the replication origin of each locus is indicated. σ^I activity in wild-type (WT) and a Δ*ponA* mutant are shown. The average copy numbers of the *amyE* and *ycgO* loci are ~1.4-times higher than the *yhdG* locus (Karaboja et al. 2021) and likely explain the ~1.4-fold reduced response of the transcriptional reporter at the *yhdG* locus.

Figure S14. Analysis of the two site-1 cleavages in RsgI. Representative immunoblots of whole cells and protoplasts of the indicated strains. All strains lack the *rsgI* gene and contain the indicate *gfp-rsgI-his* variant under xylose inducible control. Cells were grown in LB medium supplemented with 10 mM xylose to mid-exponential phase and a sample collected. The rest of the culture was treated with lysozyme in the presence of hypertonic buffer. The resulting protoplasts were washed to remove extracellular proteins that were not associated with the cytoplasmic membrane. GFP-RsgI-His cleavage products were assessed by immunoblot using anti-His and anti-GFP antibodies. The two N- and C-terminal Site-1 cleavage products are indicated with an (a) and (b). Only the (b) cleavage products stably interact and are protected from RasP-mediated Site-2 proteolysis.

Figure S15. The scrambled amino acids in the intrinsically disordered region of *B. subtilis* RsgI. **(A)** Amino acid sequences of the the native *B. subtilis* RsgI ID region and two variants in which the ordered of the amino acids were scrambled. Residues with similar properties are colored identically. **(B)** Both scrambled IDRs are predicted to be intrinsically disordered. The graphical output was from PrDOS (Ishida and Kinoshita 2007).

Figure S16. The C-terminal regions of PBP1 homologs are predicted to be intrinsically disordered. Graphical outputs from PrDOS (Ishida and Kinoshita 2007) for PBP1 homologs from *B. subtilis* 168, *B. cereus* ATCC 14579 (*B. cereus* 14), *B. cereus* B4088 (BACERE00185_03869) (*B. cereus* B4), *B. cereus* JRS1 (BN2127_JRS1_05966) (*B. cereus* JR).

Figure S17. Alignment of PBP1 homologs highlights similarities and differences in the unstructured regions. Amino acid alignment of PBP1 homologs from the Bacillaceae family. Amino acid sequences were aligned using Clustal Omega (Madeira et al. 2019) and displayed using coffee (Di Tommaso et al. 2011). Conserved residues in the cytoplasmic, transmembrane (TM), glycosyltransferase, and transpeptidase domains are shown in greyscale. Conserved residues in the fibronectin 3 (FN3)-like domain are in orange. The ten most common residues (D, E, K, R, Q, N, S, T, G, P) in the C-terminal unstructured regions are highlighted. Residues with similar properties are colored the same. The boxed region is enlarged below to show the similarities and differences among the unstructured regions.

Figure S18. The IDR on PBP1 is important for function. (A) Spot dilutions on LB agar plates supplemented with 100 or 15 μM IPTG. The first strain is wild-type (WT) the second lacks all 4 aPBP genes (Δ4). All other strains lack the four aPBP genes and harbor the indicated variant of *ponA* expressed under IPTG control. The *ponA* variant lacking its ID region is labeled ΔID. Those with a different IDR appended onto *ponA*ΔID are labeled with the source of the IDR. The strains with *ponA*ΔID and *ponA*ΔID fused to the folded extracytoplasmic domain from SpoIVFA (4FA) grow less will with 15 μM IPTG. Below the spot-dilutions is a Bocillin gel of the same strains grown in the presence of 15 μM IPTG. **(B)** Bar graph showing β-galactosidase activity from a σ^I-responsive reporter in the indicated strains grown in LB with 15 μM IPTG. Error bars represent standard deviation from three biological replicates.

Figure S19. The IDR on PBP1 is important for function. Representative phase-contrast and fluorescence images of cells expressing wild-type PBP1, the variant lacking its IDR, replaced with the IDR from *B. subtilis* RsgI, or the extracytoplasmic domain of SpoIVFA (ECD4FA). All four strains lack their native aPBPs. Cells

were grown in LB medium supplemented with 15 μM IPTG. Lysed cells (yellow carets) and cell with morphological defects (white carets) are highlighted.

Figure S20. The IDR on PBP1 is important for function. Spot dilutions of the indicated strains on LB agar plates supplemented with IPTG. Below the spot-dilutions are Bocillin gels of the *gpsB*+ versions of the strains used above them. Even in the presence of 250 μM IPTG the *ponA* variants lacking its IDR and the chimera with the folded extracellular domain of SpoIVFA (4FA) are growth impaired.

Figure S21. The IDR on PBP1 is important for function. Representative phase-contrast and fluorescence images of cells expressing wild-type PBP1, the variant lacking its IDR, or replaced with the indicated IDRs or folded domain. All strains lack the four native aPBP genes and *gpsB* and constitutively express cytoplasmic GFP. Cells were grown in LB medium supplemented with 25 μM IPTG.

Figure S22. An intrinsically disordered region on PBP1 is important for function. (A) Amino acid sequences of the the native IDR of PBP1 and two variants in which the order of the amino acids were scrambled. Residues with similar properties are colored identically. **(B)** Both scrambled IDRs are predicted to be intrinsically disordered. Graphical output from PrDOS (Ishida and Kinoshita 2007). **(C)** Spot dilutions of the indicated strains on LB agar plates supplemented with IPTG. Both scrambled IDRs function similarly to wild-type. **(D)** Bar graph showing β-galactosidase activity from a σ^I-responsive reporter in the indicated strains grown in LB with 50 μM IPTG. Error bars represent standard deviation from three biological replicates.

Figure S23. Cell expressing PBP1 without its intrinsically disordered region induce σ^I even under conditions where growth is not impaired. (A) Spot dilutions of the indicated strains on LB agar plates supplemented with IPTG. All strains contain native *pbp4*, *pbpF*, and *pbpG*. The only gene deletion is *ponA*. **(B)** Bocillin gel of the same strains shown in A. **(C)** Bar graph showing β-galactosidase activity from the σ^I-responsive reporter P(bcrC)-*lacZ* in the indicated strains grown in LB with 25 or 50 μM IPTG. Error bars represent standard deviation from three biological replicates.

S1 Table *Bacillus subtilis* strains used in this study. All strains, their genotypes, and sources are listed in this table.

S2 Table Plasmids used in this study. All plasmids and their sources are listed in this table.

S3 Table Oligonucleotide primers used in this study. All oligonucleotides used for plasmid construction, gene deletion, or sequencing are listed in this table.

S4 Table RsgI homologs. NCBI Reference numbers and species for all RsgI homologs in the alignment in Figure S7.

SUPPLEMENTAL REFERENCES

Di Tommaso P, Moretti S, Xenarios I, Orobitg M, Montanyola A, Chang JM, Taly JF, Notredame C. 2011. T-Coffee: a web server for the multiple sequence alignment of protein and RNA sequences using structural information and homology extension. *Nucleic Acids Res* **39**: W13-17.

Erdos G, Pajkos M, Dosztanyi Z. 2021. IUPred3: prediction of protein disorder enhanced with unambiguous experimental annotation and visualization of evolutionary conservation. *Nucleic Acids Res* **49**: W297-W303.

Gibson DG. 2011. Enzymatic assembly of overlapping DNA fragments. *Methods Enzymol* **498**: 349-361.

Ishida T, Kinoshita K. 2007. PrDOS: prediction of disordered protein regions from amino acid sequence. *Nucleic Acids Res* **35**: W460-464.

Jones DT, Cozzetto D. 2015. DISOPRED3: precise disordered region predictions with annotated protein-binding activity. *Bioinformatics* **31**: 857-863.

Karaboja X, Ren Z, Brandao HB, Paul P, Rudner DZ, Wang X. 2021. XerD unloads bacterial SMC complexes at the replication terminus. *Mol Cell* **81**: 756-766 e758.

Koo BM, Kritikos G, Farelli JD, Todor H, Tong K, Kimsey H, Wapinski I, Galardini M, Cabal A, Peters JM et al. 2017. Construction and Analysis of Two Genome-Scale Deletion Libraries for Bacillus subtilis. *Cell Syst* **4**: 291-305 e297.

Madeira F, Park YM, Lee J, Buso N, Gur T, Madhusoodanan N, Basutkar P, Tivey ARN, Potter SC, Finn RD et al. 2019. The EMBL-EBI search and sequence analysis tools APIs in 2019. *Nucleic Acids Res* **47**: W636-W641.

Meeske AJ, Sham LT, Kimsey H, Koo BM, Gross CA, Bernhardt TG, Rudner DZ. 2015. MurJ and a novel lipid II flippase are required for cell wall biogenesis in Bacillus subtilis. *Proc Natl Acad Sci U S A* **112**: 6437-6442.

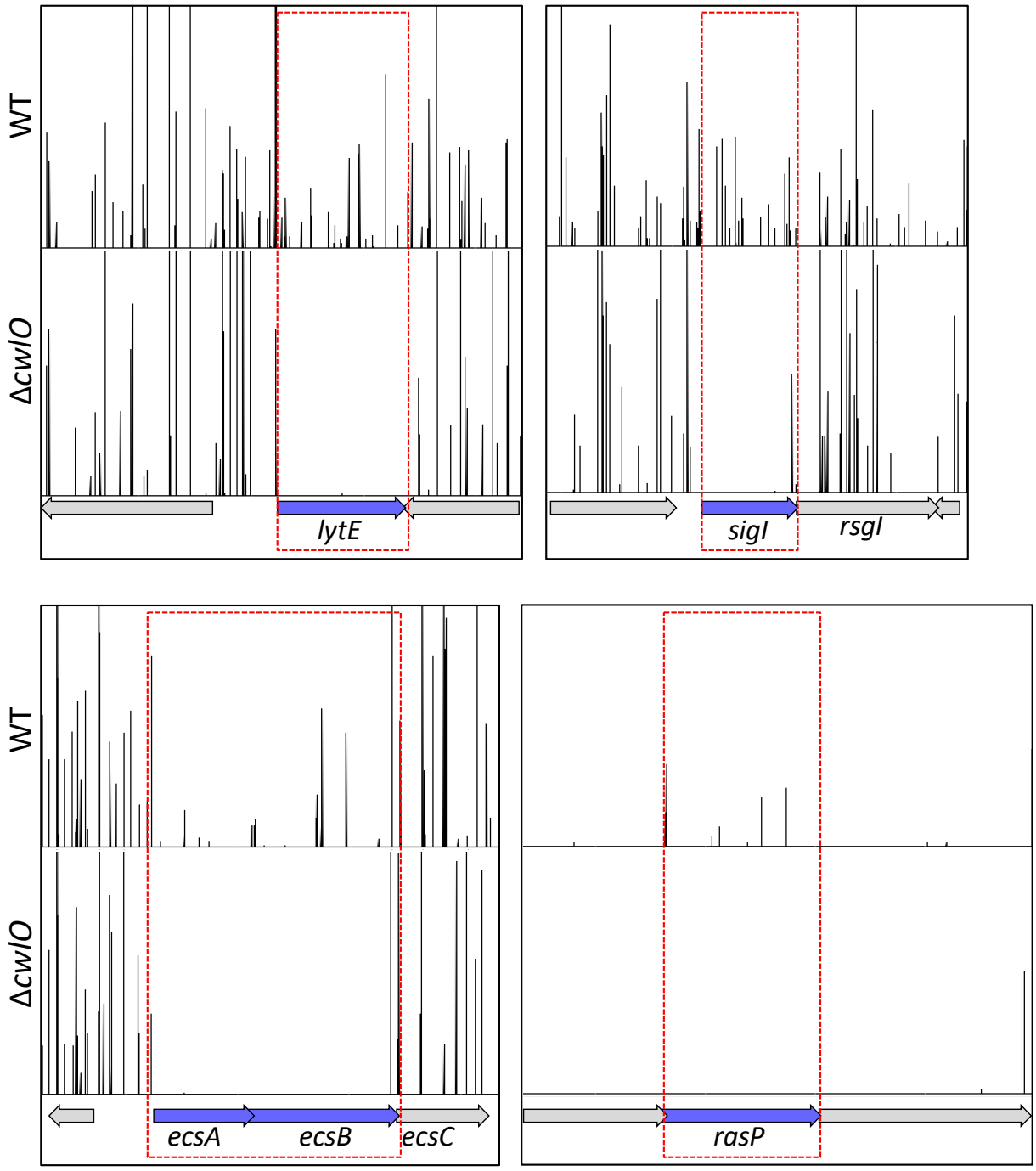

Figure S1. Transposon-sequencing identifies *rasP*, *ecsA,* and *ecsB* as synthetic lethal with *cwlO*.
Transposon insertion profiles from wild-type (WT) and Δ*cwlO* libraries. Four regions of the genome are shown. Each vertical line indicates a transposon insertion site; the height reflects the number of sequencing reads at this position. Transposon insertions in *lytE*, *sigI*, *rasP*, *ecsA* and *ecsB* were under-represented in the Δ*cwlO* Tn library compared to wild-type. Maximum reads were normalized to 150 for regions containing *lytE, cwlO*, and *ecsAB*, and 50 for the region with *rasP*.

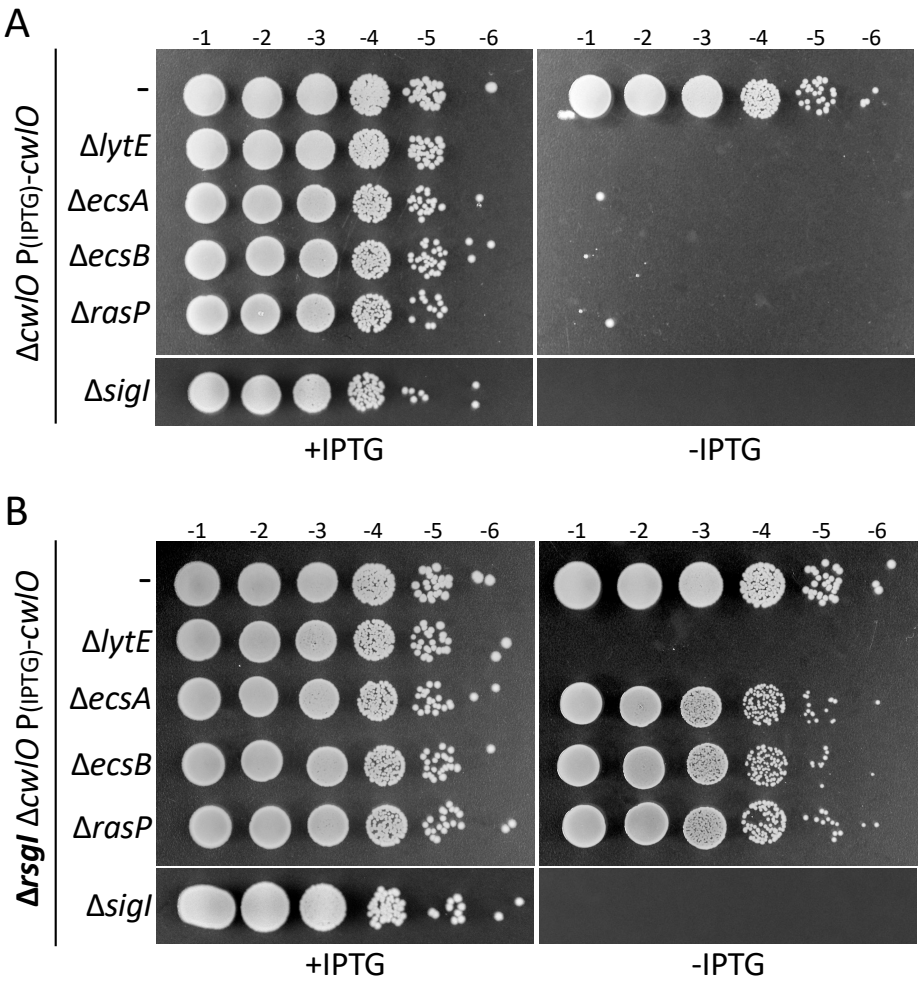

Figure S2. *rasP*, *ecsA* and *ecsB* are synthetic lethal with *cwlO.*
(A) Validation of the Tn-seq data using an IPTG-regulated allele of *cwlO*. **(B)** Synthetic lethality can be suppressed by Δ*rsgI*. Spot-dilutions of the indicated strains in the presence and absence of 500 µM IPTG. All strains were grown in the presence of inducer to OD600 ~2.0. The cultures were washed without inducer, resuspended to an OD600 of 1.5, and 10-fold serially diluted. Five microliters of each dilution were spotted onto LB agar plates with and without IPTG. The plates for photographed after overnight incubation at 37 ˚C. The synthetic lethality between *sigI* and *rasP*, *ecsA*, and *ecsB* can be suppressed by Δ*rsgI*, placing these genes upstream of the anti-sigma factor.

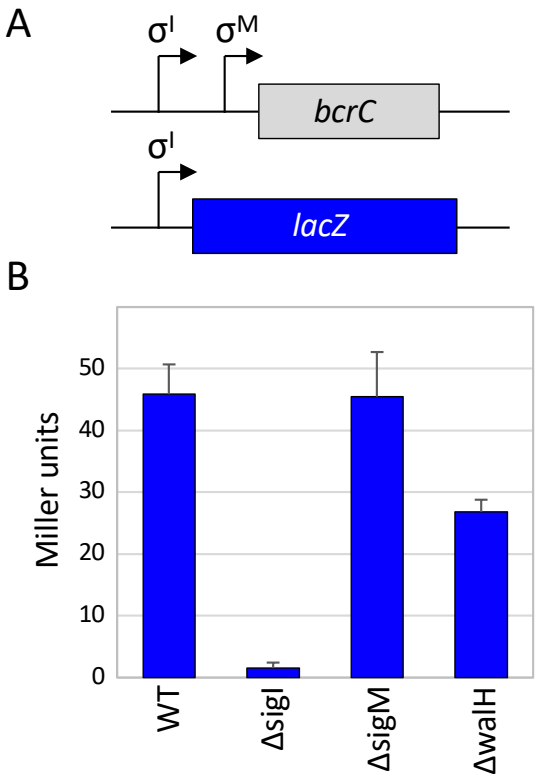

Figure S3. The σ^{I}-responsive *bcrC* promoter-fusion to *lacZ* is specific to σ^{I}.
(A) Schematic diagram of the *bcrC* promoter region and the σ^{I}-responsive promoter fusion used in this study. **(B)** Bar graph showing β-galactosidase activity from the P(bcrC)-*lacZ* reporter in the indicated strains. The Δ*walH* mutation results in high WalR activity. Activity was assayed in exponentially growing cultures in LB. Error bars represent standard deviation from three biological replicates.

Figure S4
Brunet et al.

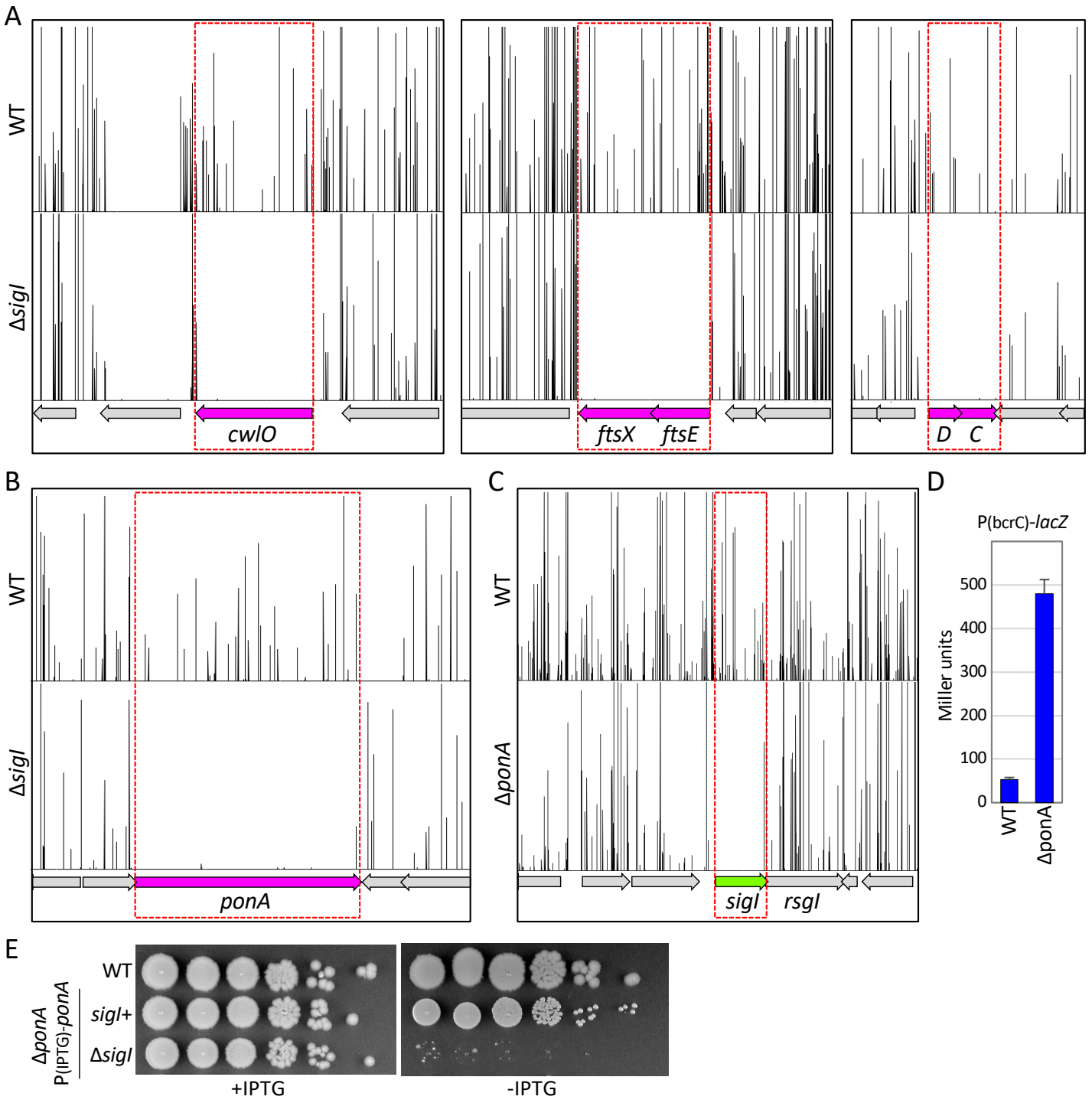

Figure S4. Transposon-sequencing identifies *ponA* and *sigI* as a synthetic lethal pair.
(A-B) Transposon insertion profiles from transposon libraries generated in wild-type (WT) and in the Δ*sigI* mutant. Four genomic regions are shown. The height of each line reflects the number of sequencing reads that map to this position. Tn insertions in *cwlO*, *ftsEX*, *sweDC* and *ponA* are underrepresented in the Δ*sigI* Tn library compared to wild-type. **(C)** Transposon insertion profiles from Tn libraries generated in wild-type (WT) and in a Δ*ponA* P(IPTG)-*ponA* mutant (Δ*ponA*) in the absence of IPTG. Tn insertions in *sigI* are underrepresented in the Δ*ponA* library compared to wild-type. (**D**) σ^I activity is increased in the Δ*ponA* mutant. Bar graph showing β-galactosidase activity from the σ^I-responsive P(bcrC)-*lacZ* reporter in the indicated strains. Activity was assayed in exponentially growing cultures in LB. Error bars represent standard deviation from three biological replicates. (**E**) Validation of Tn-seq results. Spot dilutions of the indicated strains in the presence and absence of inducer (IPTG).

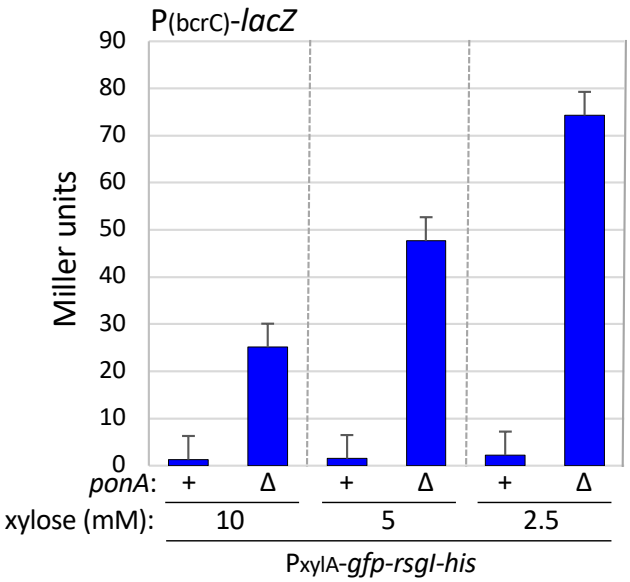

Figure S5. Functionality of the GFP-RsgI-His fusion.
Bar graph showing β-galactosidase activity from the σ^{I}-responsive P(bcrC)-*lacZ* reporter in the presence (+) and absence (Δ) of *ponA* in the Δ*rsgI* mutant complemented by a xylose-inducible *gfp-rsgI-his* allele. Activity was assayed in exponentially growing cultures in LB supplemented with the indicated concentrations of xylose (in mM). Error bars represent standard deviation from three biological replicates.

Figure S6
Brunet et al.

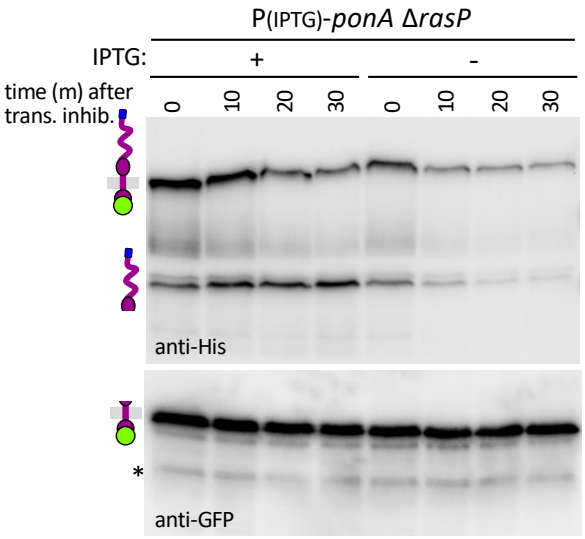

Figure S6. Intramembrane cleavage of RsgI in response to PBP1 depletion requires RasP. Representative immunoblots showing the stability of GFP-RsgI-His cleavage products in the indicated strains that lack the native rsgI gene and harbor a xylose-regulated allele of gfp-rsgI-his. Cells were grown in LB medium supplemented with 20 mM xylose and 50 µM IPTG. The cells were then washed to remove IPTG and grown for 1.5 hours in LB medium with 20 mM xylose to deplete PBP1. At mid-exponential phase they were treated with spectinomycin and chloramphenicol to inhibit protein synthesis. Samples were collected at the indicated time points (in min) before and after addition of antibiotics and GFP-RsgI-His was assessed by immunoblot using anti-His and anti-GFP antibodies. Upon depletion of PBP1, the membrane-anchored site-1 cleavage product was stable over the time course, indicating that further processing requires RasP. By contrast the extracytoplasmic site-1 cleavage product was unstable, presumably due to release into the culture supernatant.

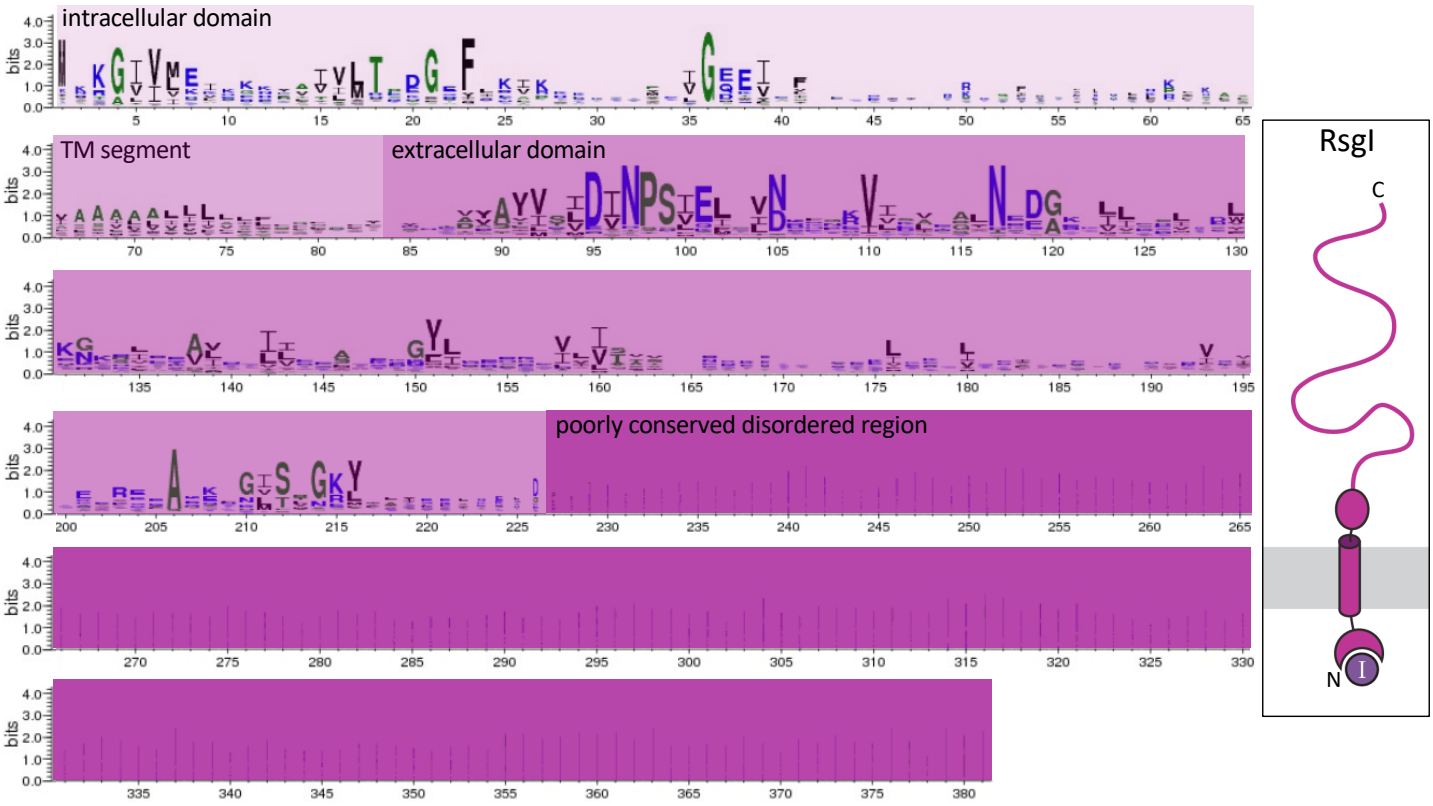

Figure S7. Multiple sequence alignment of RsgI homologs displayed as a WebLogo. Intracellular domain, transmembrane (TM) segment, extracellular domain, and the poorly conserved disordered region are shown in different shades of purple. Schematic representation of RsgI bound to σ^I (I) is shown on the right.

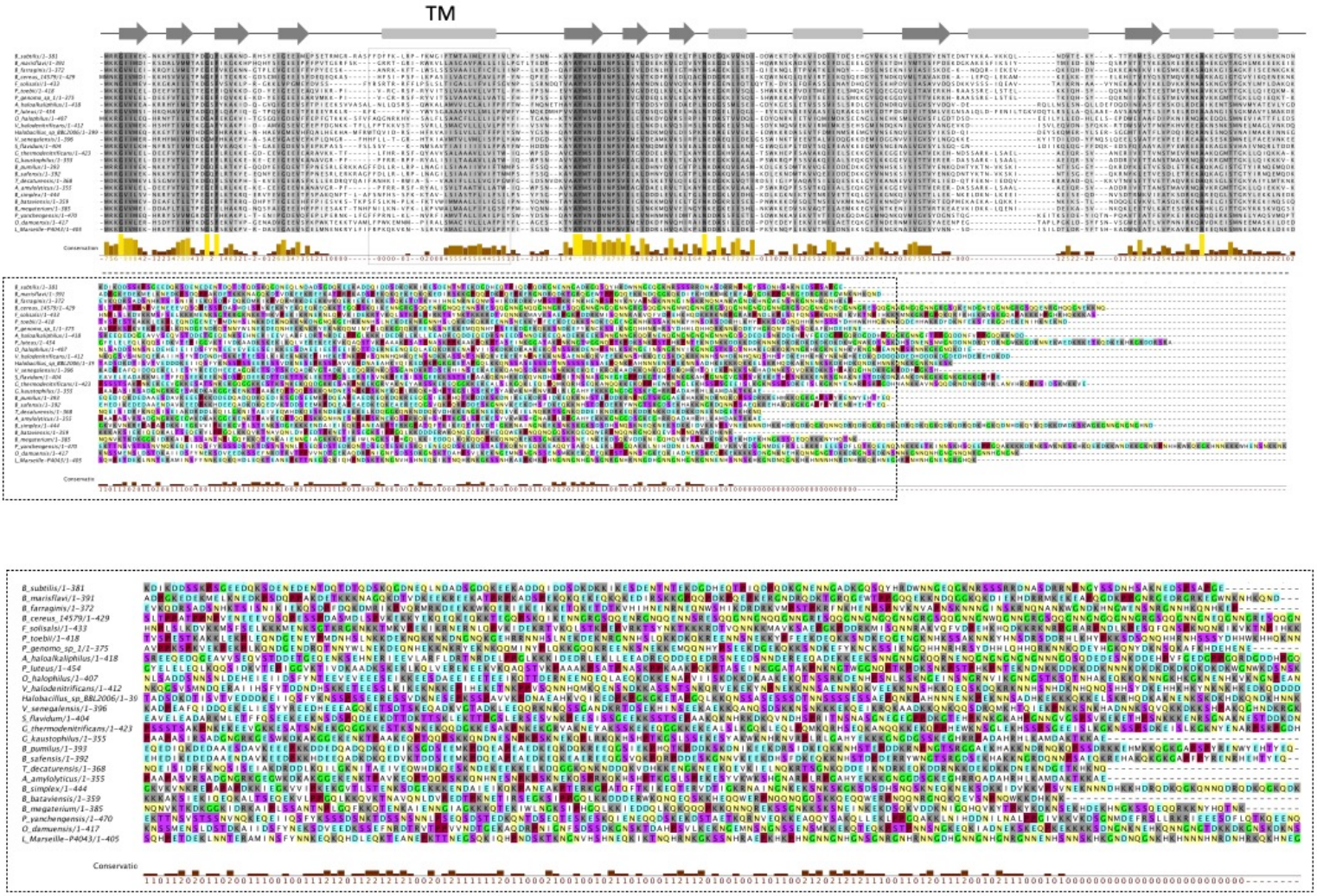

Figure S8. Alignment of RsgI homologs highlights similarities and differences in the unstructured region. Amino acid alignment of of RsgI homologs from the Bacillaceae family. Amino acid sequences were aligned using Clustal Omega (Madeira et al., 2019) and displayed using T-coffee (Di Tommaso et al., 2011). Conserved residues in the cytoplasmic domain, transmembrane (TM) segment, and the extracytoplasmic juxta-membrane domain are shown in greyscale. The ten most common residues (D/E, K/R, Q/N, S/T, G, P) in the C-terminal unstructured regions are highlighted. Residues with similar properties are colored the same. The boxed region is enlarged below to highlight the similarities and differences among the unstructured regions. The NCBI reference sequence for each RsgI homolog can be found in Table S4.

PrDOS (**Pr**otein **D**is**O**rder prediction **S**ystem)

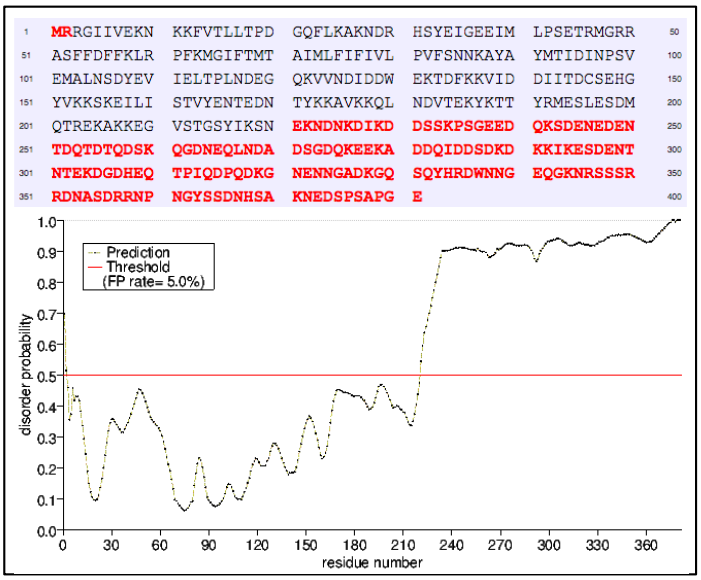

DISOPRED3 (Protein Intrinsic Disorder Prediction)

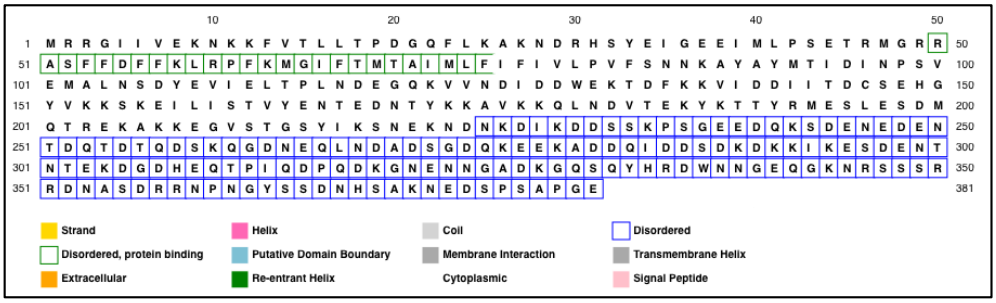

IUPred3 (**Pred**iction of **I**ntrinsically **U**nstructured Proteins)

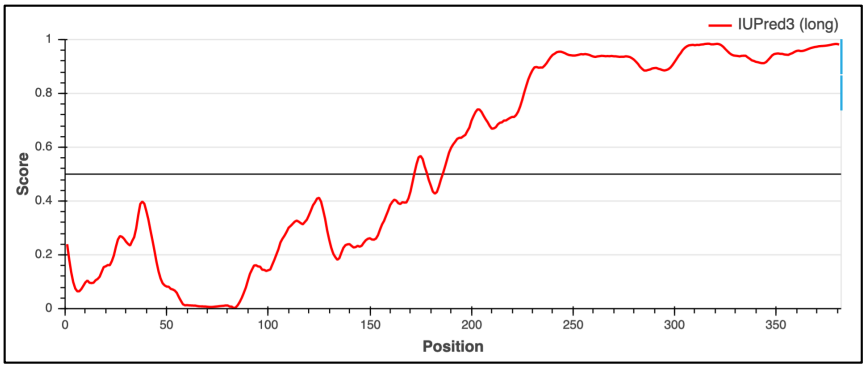

Figure S9. The C-terminal region of RsgI is predicted to be intrinsically disordered. Graphical outputs from the indicated prediction programs of intrinsic disorder (Erdos et al., 2021; Ishida & Kinoshita, 2007; Jones & Cozzetto, 2015; Madeira et al., 2019). All three programs predict that the C-terminal ~160 residues of RsgI are intrinsically disordered.

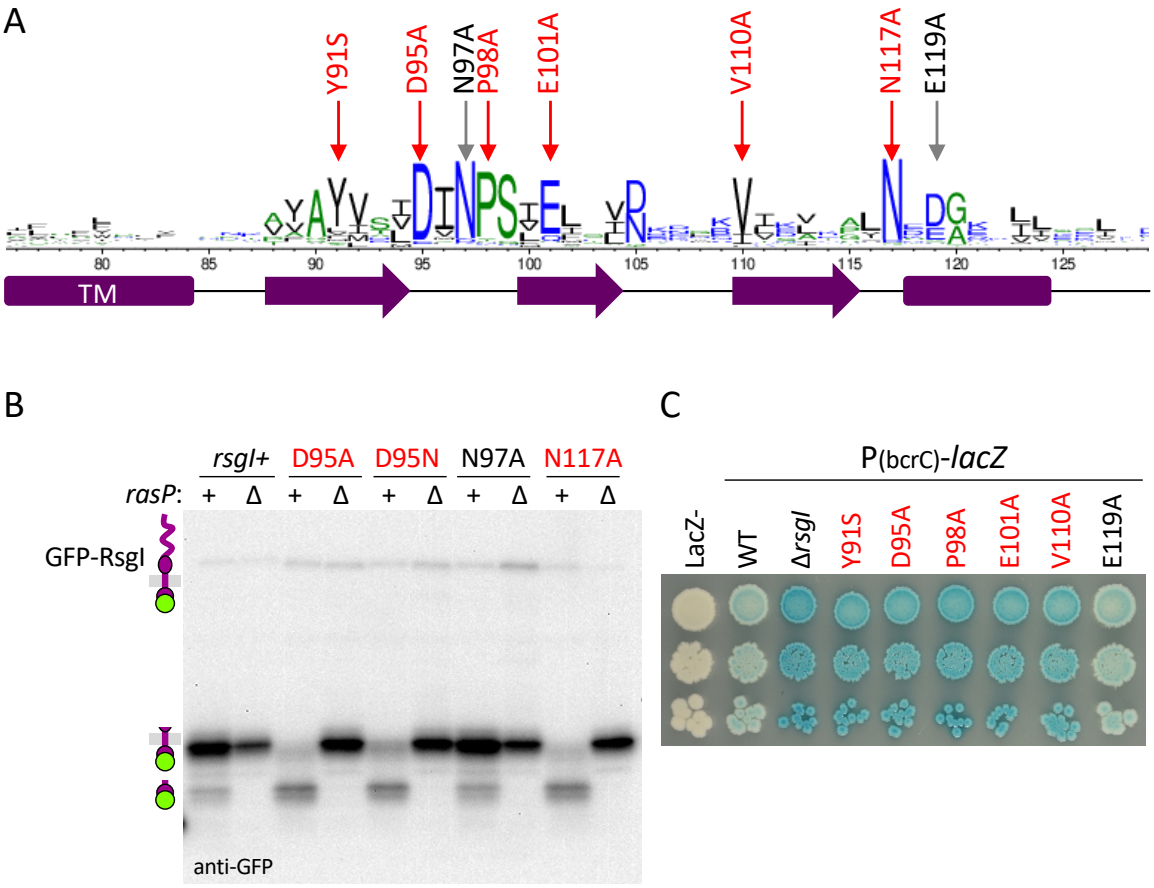

Figure S10. The juxta-membrane domain of RsgI is required for regulated proteolysis.
(A) Multiple sequence alignment using WebLogo of the TM segment and part of the juxta-membrane domain of RsgI. Below the alignment are predicted secondary structure elements. Amino acid substitutions tested are highlighted above the alignment. Those in red were constitutively cleaved and phenocopied a Δ*rsgI* mutant. **(B)** Immunoblot analysis of GFP-RsgI in the indicated RsgI mutants in the presence and absence of *rasP*. **(C)** Spot dilutions of the indicated mutants harboring the σ^I-responsive P(bcrC)-*lacZ* reporter on LB agar supplemented with X-gal. The strains used in panel C contained *rsgI* that lack GFP- and His-tags.

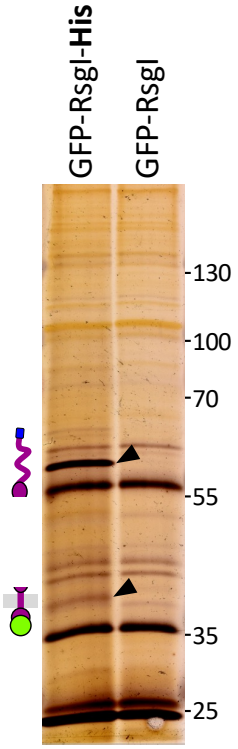

Figure S10. Site-1-cleaved RsgI products remain associated.
Silver-stained gel of elutions from anti-His immunoprecipitation of GFP-RsgI-His from detergent-solubilized membrane fractions of *B. subtilis* cells expressing GFP-RsgI-His or GFP-RsgI. Black carets highlight the N- and C-terminal site-1 cleavage products identified by mass spectrometry. Molecular weight markers (in kDa) are shown.

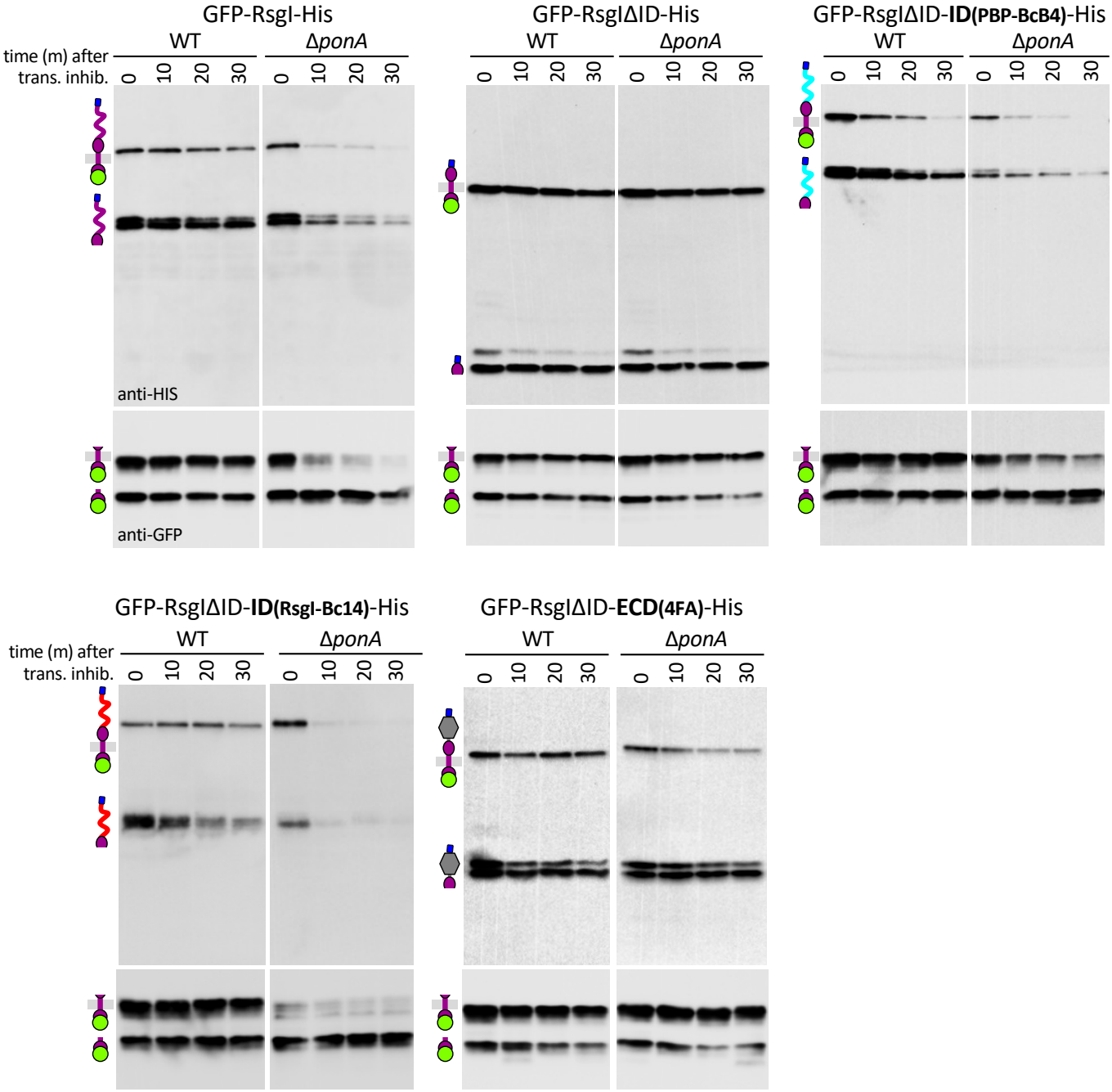

Figure S12. Intrinsically disordered regions from *B. cereus* RsgI homologs function in place of the IDR on *B. subtilis* RsgI. Representative immunoblots showing the stability of GFP-RsgI-His cleavage products in the indicated strains. All strains lack the native *rsgI* gene and harbor the indicated variants under xylose-inducible control. Cells were grown in LB medium supplemented with 10 mM xylose to mid-exponential phase and then treated with spectinomycin and chloramphenicol to inhibit protein synthesis. Samples were collected at the indicated time points (in min) before and after addition of antibiotics and GFP-RsgI-His variants were analyzed by immunoblot using anti-His and anti-GFP antibodies.

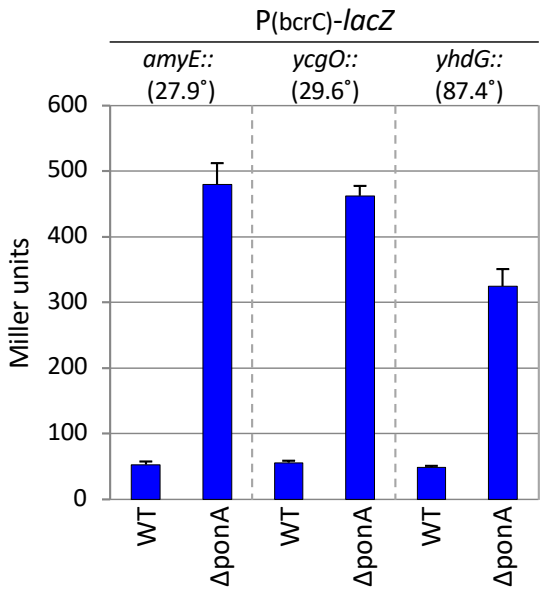

Figure S13. The chromosomal insertion site of the P(bcrC)-*lacZ* reporter influences the magnitude of the response. Bar graph showing β-galactosidase activity from the σ^{I}-responsive reporter P(bcrC)-*lacZ* integrated at three chromosomal locations (*amyE*, *ycgO*, and *yhdG*). The location in degrees relative to the replication origin of each locus is indicated. σ^{I} activity in wild-type (WT) and a Δ*ponA* mutant are shown. The average copy numbers of the *amyE* and *ycgO* loci are ~1.4-times higher than the *yhdG* locus (Karaboja et al., 2021) and likely explain the ~1.4-fold reduced response of the transcriptional reporter at the *yhdG* locus.

Figure S14
Brunet et al.

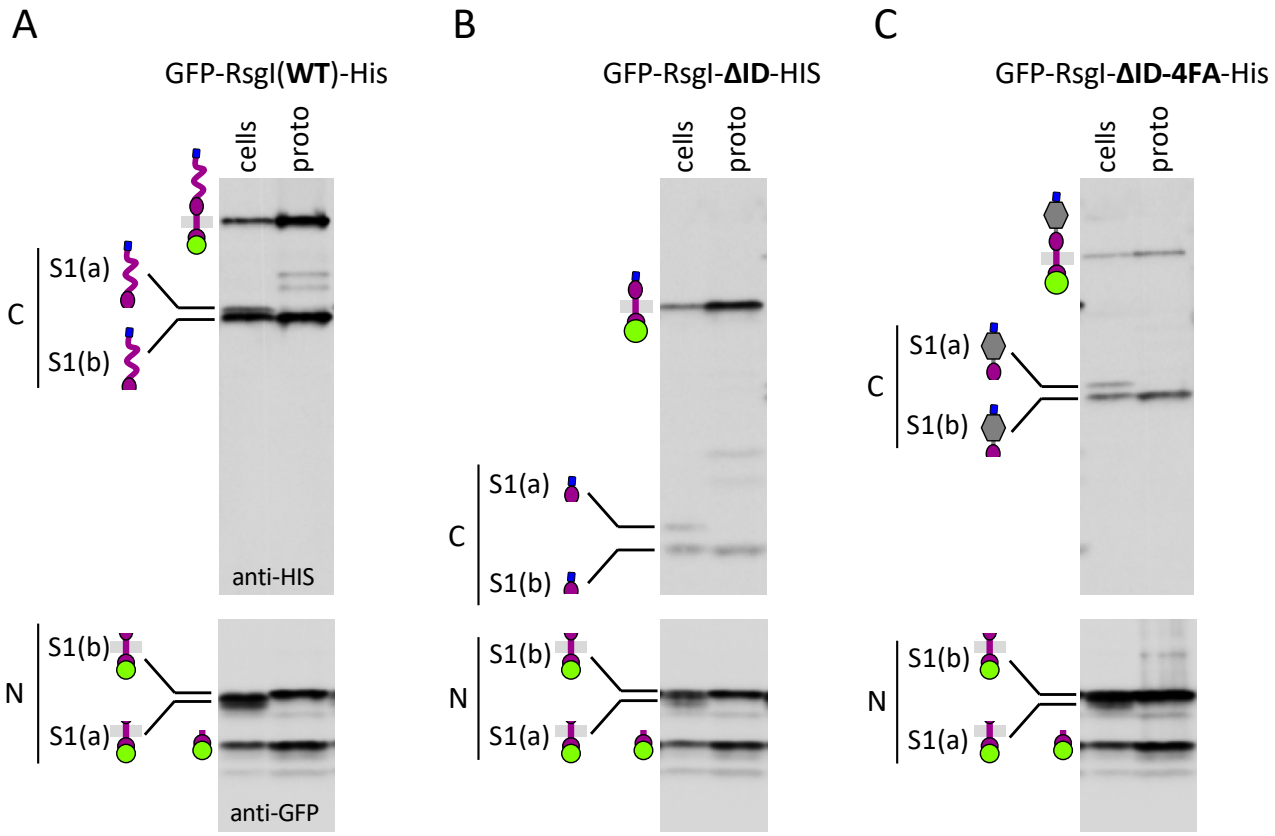

Figure S14. Analysis of the two site-1 cleavages in RsgI. Representative immunoblots of whole cells and protoplasts of the indicated strains. All strains lack the *rsgI* gene and contain the indicate *gfp-rsgI-his* variant under xylose inducible control. Cells were grown in LB medium supplemented with 10 mM xylose to mid-exponential phase and a sample collected. The rest of the culture was treated with lysozyme in the presence of hypertonic buffer. The resulting protoplasts were washed to remove extracellular proteins that were not associated with the cytoplasmic membrane. GFP-RsgI-His cleavage products were assessed by immunoblot using anti-His and anti-GFP antibodies. The two N- and C-terminal Site-1 cleavage products are indicated with an (a) and (b). Only the (b) cleavage products stably interact and are protected from RasP-mediated Site-2 proteolysis.

A

RsgI-WT (*B. subtilis*)

KDIKDDSSKPSGEEDQKSDENEDENTDQTDTQDSKQGDNEQLNDADSGDQKEEKADDQIDDSDKDKKIKES
DENTNTEKDGDHEQTPIQDPQDKGNENNGADKGQSQYHRDWNNGEQGKNRSSSRRDNASDRRNPNGYSSDN
HSAKNEDSPSAPGE

RsgI-scramble1 (*B. subtilis*)

DQNENDTESEKKNSSSPKGKQIQDADRAEDNAPPENHRDDPDNDQQDLGDTNDNGDDYQKGEQDKKSDDRK
DDRPADSEISDESNYSANQSGDGAQEDSKGSRNDSQKGSRHENKGISQTTESKWNESDEHPNGTDQIEGKD
QNTKNNEDESKDKD

RsgI-scramble2 (*B. subtilis*)

SADDDPSPDREDKNALKNQQDYAEDSSKNDDGENGTKINQKQNSSGDNDKQSENTNEDQDSPITQHYERDE
SSSDNEKDNRDWKKHGNDDKGSGEQQRGDEDDGPSDKDAHNSPQNKQSRSRASDGSEDKTAKGGEPKDEEN
QEEITQDKDDITNN

B

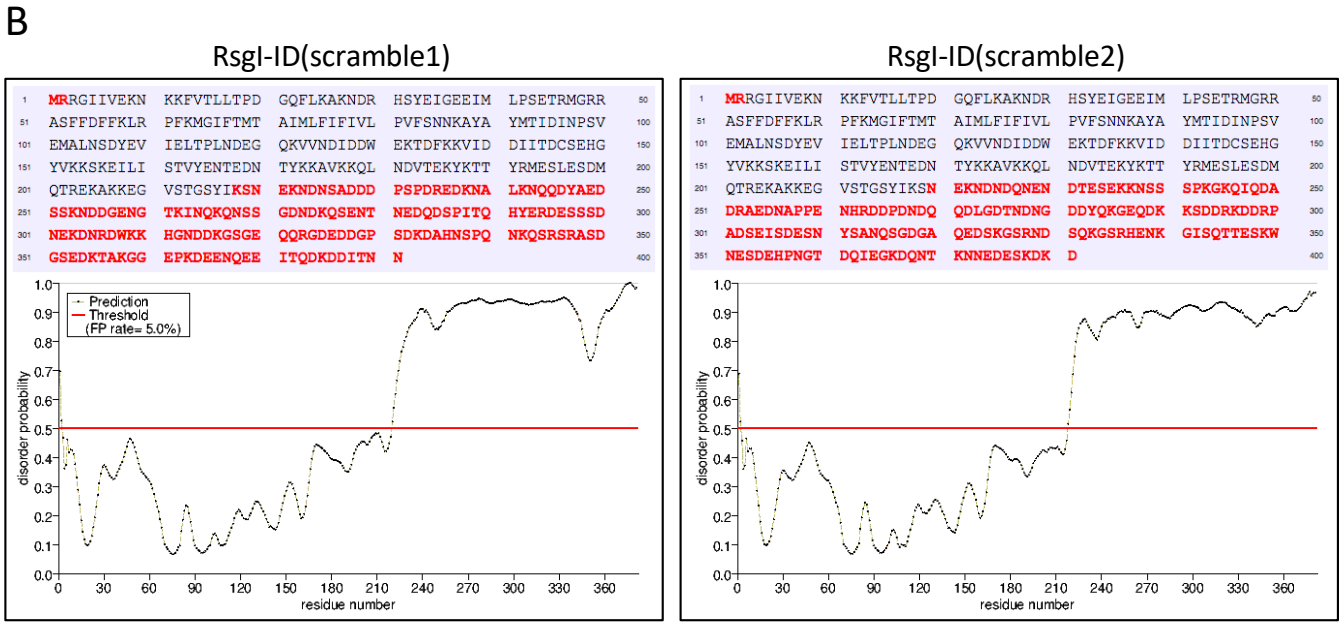

Figure S15. The scrambled amino acids in the intrinsically disordered region of *B. subtilis* RsgI.
(A) Amino acid sequences of the the native *B. subtilis* RsgI ID region and two variants in which the ordered of the amino acids were scrambled. Residues with similar properties are colored identically. **(B)** Both scrambled IDRs are predicted to be intrinsically disordered. The graphical output was from PrDOS (Ishida & Kinoshita, 2007).

Figure S16
Brunet et al.

PBP1 (*B. subtilis*)

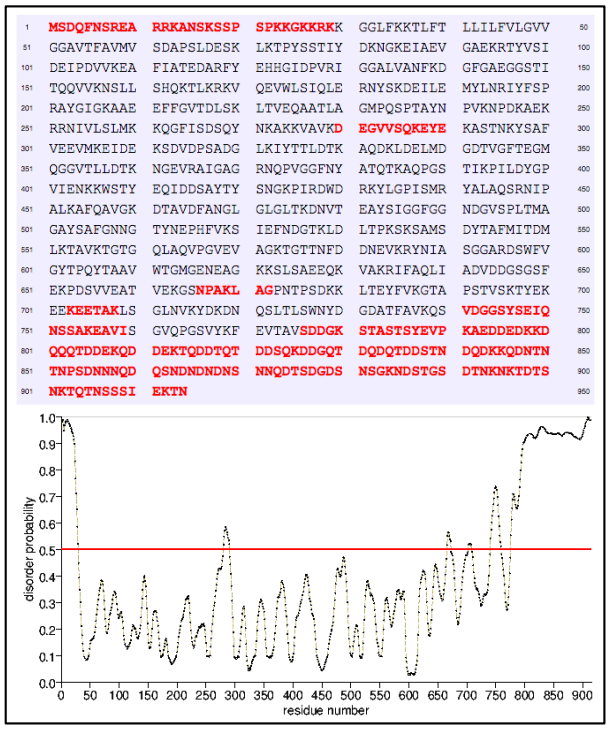

PBP1 (*B. cereus* 14)

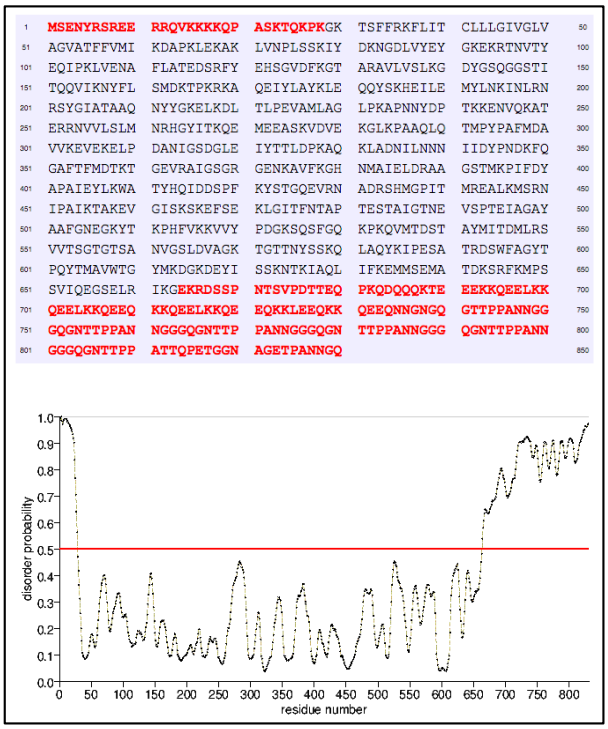

PBP1 (*B. cereus* B4)

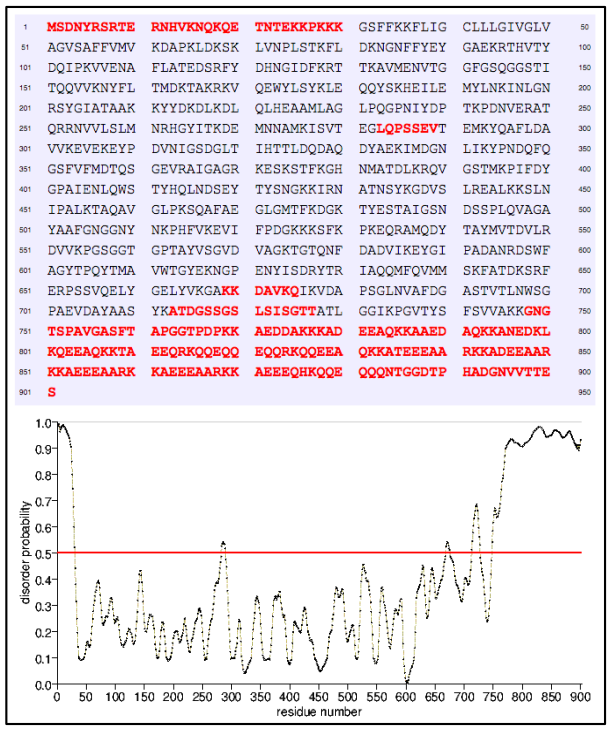

PBP1 (*B. cereus* JR)

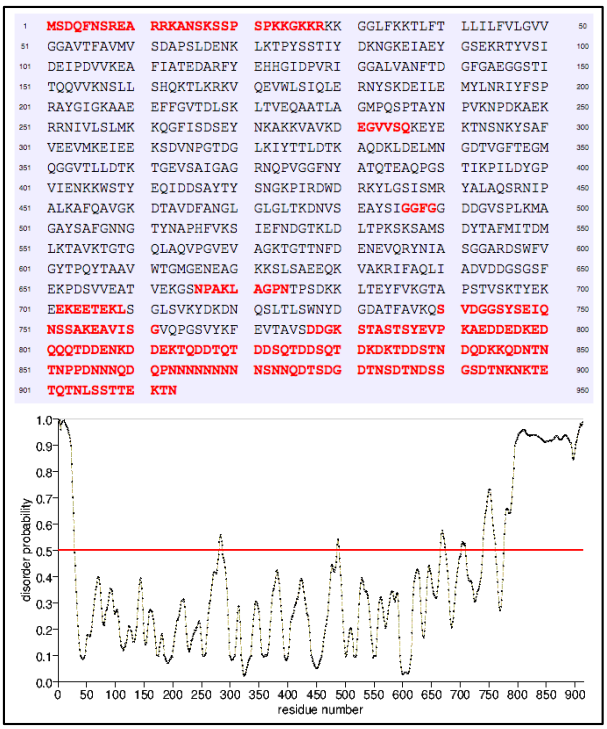

Figure S16. The C-terminal regions of PBP1 homologs are predicted to be intrinsically disordered. Graphical outputs from PrDOS (Ishida & Kinoshita, 2007) for PBP1 homologs from *B. subtilis* 168, *B. cereus* ATCC 14579 (*B. cereus* 14), *B. cereus* B4088 (BACERE00185_03869) (*B. cereus* B4), *B. cereus* JRS1 (BN2127_JRS1_05966) (*B. cereus* JR).

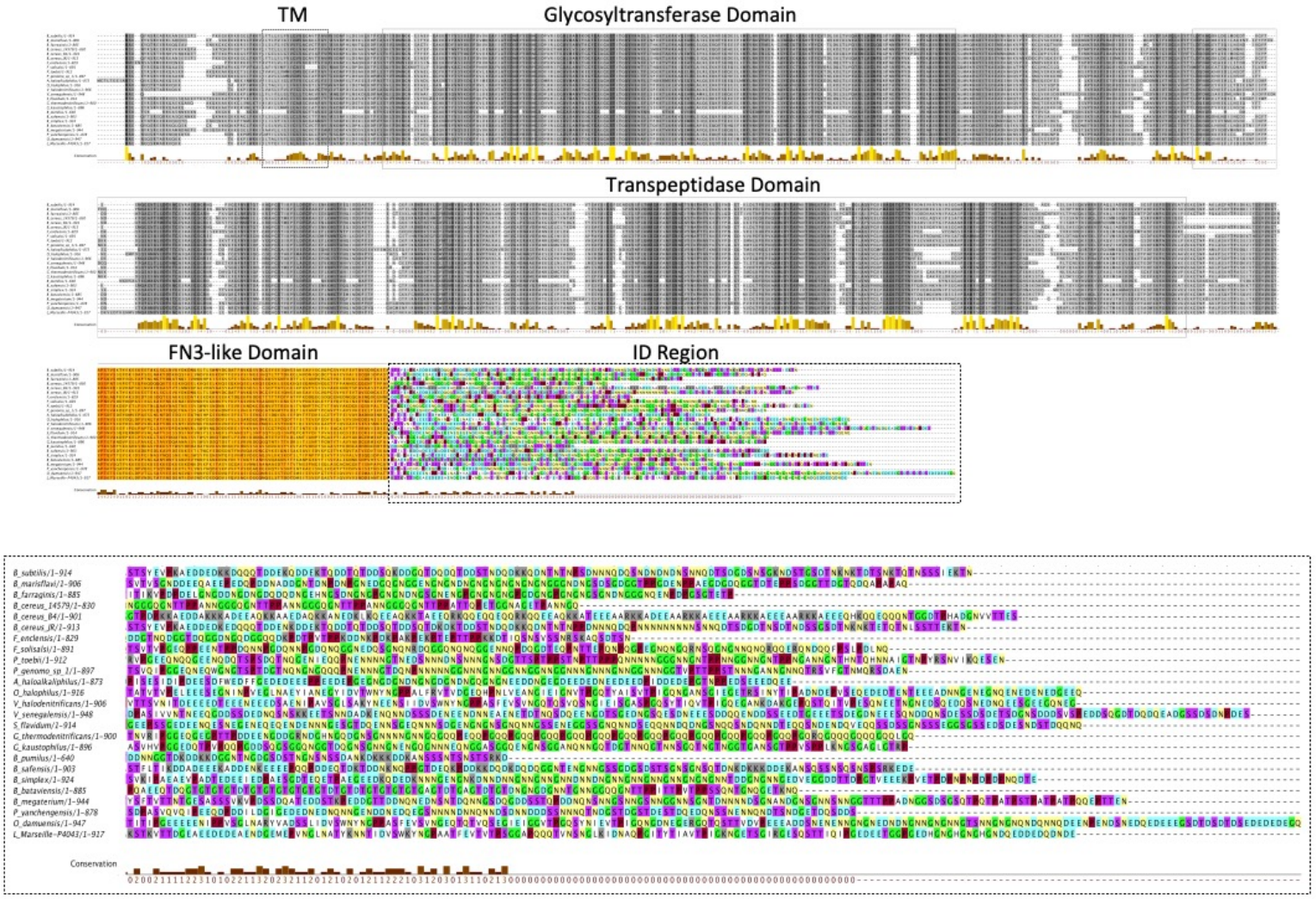

Figure S17. Alignment of PBP1 homologs highlights similarities and differences in the unstructured regions. Amino acid alignment of PBP1 homologs from the Bacillaceae family. Amino acid sequences were aligned using Clustal Omega (Madeira et al., 2019) and displayed using coffee (Di Tommaso et al., 2011). Conserved residues in the cytoplasmic, transmembrane (TM), glycosyltransferase, and transpeptidase domains are shown in greyscale. Conserved residues in the fibronectin 3 (FN3)-like domain are in orange. The ten most common residues (D, E, K, R, Q, N, S, T, G, P) in the C-terminal unstructured regions are highlighted. Residues with similar properties are colored the same. The boxed region is enlarged below to show the similarities and differences among the unstructured regions.

Figure S18
Brunet et al.

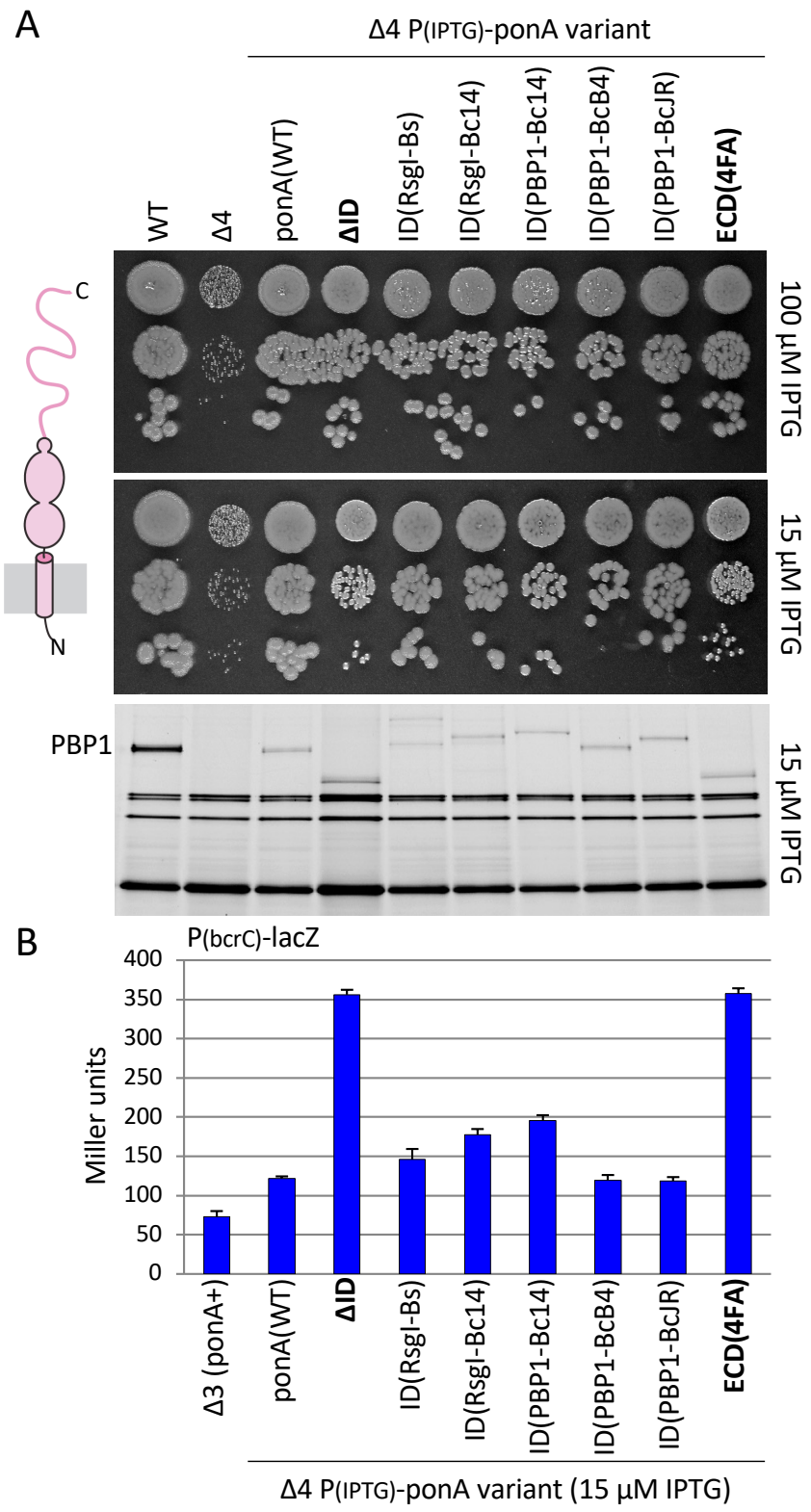

Figure S18. The IDR on PBP1 is important for function. (A) Spot dilutions on LB agar plates supplemented with 100 or 15 μM IPTG. The first strain is wild-type (WT) the second lacks all 4 aPBP genes (Δ4). All other strains lack the four aPBP genes and harbor the indicated variant of *ponA* expressed under IPTG control. The *ponA* variant lacking its ID region is labeled ΔID. Those with a different IDR appended onto *ponA*ΔID are labeled with the source of the IDR. The strains with *ponA*ΔID and *ponA*ΔID fused to the folded extracytoplasmic domain from SpoIVFA (4FA) grow less will with 15 μM IPTG. Below the spot-dilutions is a Bocillin gel of the same strains grown in the presence of 15 μM IPTG. **(B)** Bar graph showing β-galactosidase activity from a σ^I-responsive reporter in the indicated strains grown in LB with 15 μM IPTG. Error bars represent standard deviation from three biological replicates.

Figure S19
Brunet et al.

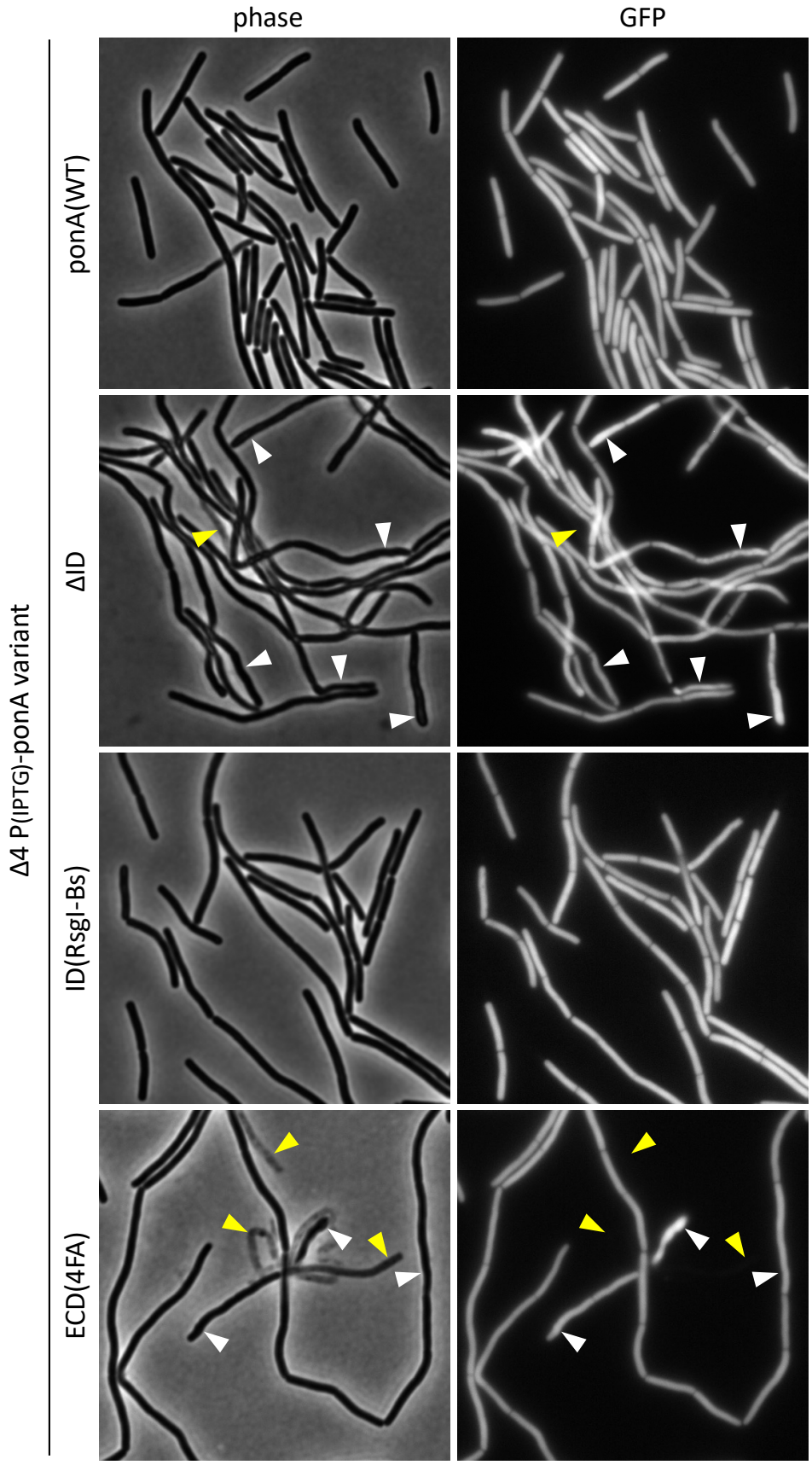

Figure S19. The IDR on PBP1 is important for function. Representative phase-contrast and fluorescence images of cells expressing wild-type PBP1, the variant lacking its IDR, replaced with the IDR from *B. subtilis* RsgI, or the extracytoplasmic domain of SpoIVFA (ECD4FA). All four strains lack their native aPBPs. Cells were grown in LB medium supplemented with 15 µM IPTG. Lysed cells (yellow carets) and cell with morphological defects (white carets) are highlighted.

Figure S20
Brunet et al.

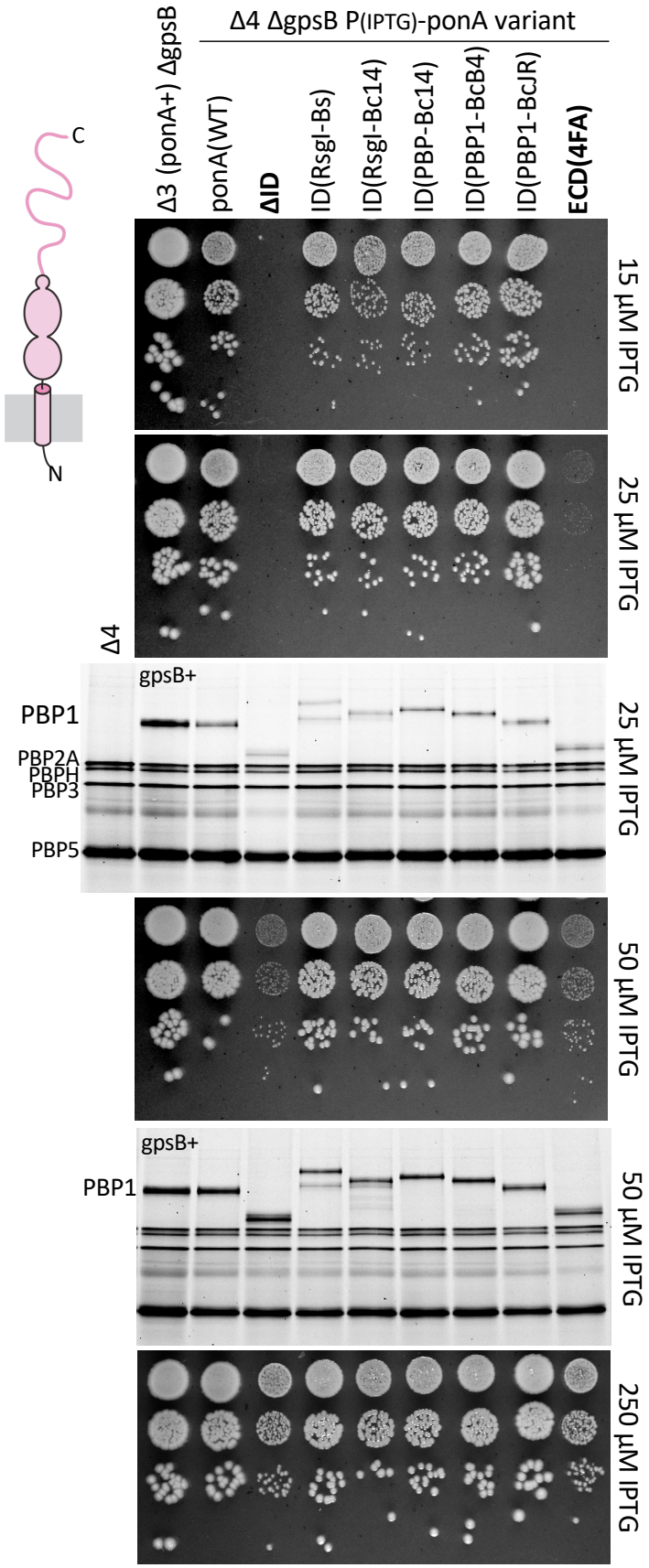

Figure S20. The IDR on PBP1 is important for function. Spot dilutions of the indicated strains on LB agar plates supplemented with IPTG. Below the spot-dilutions are Bocillin gels of the *gpsB*+ versions of the strains used above them. Even in the presence of 250 μM IPTG the *ponA* variants lacking its IDR and the chimera with the folded extracellular domain of SpoIVFA (4FA) are growth impaired.

Figure S21
Brunet et al.

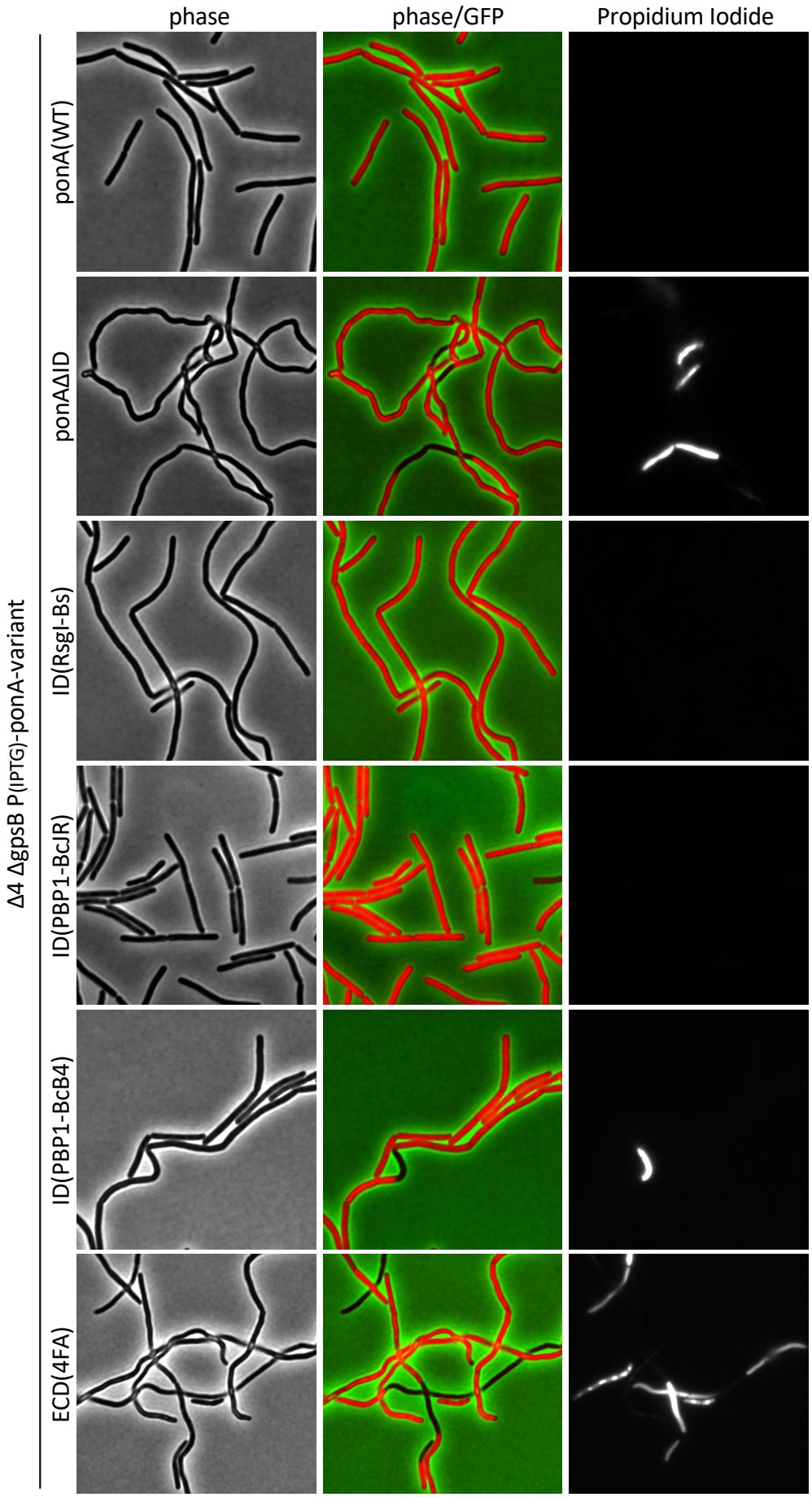

Figure S21. The IDR on PBP1 is important for function. Representative phase-contrast and fluorescence images of cells expressing wild-type PBP1, the variant lacking its IDR, or replaced with the indicated IDRs or folded domain. All strains lack the four native aPBP genes and *gpsB* and constitutively express cytoplasmic GFP. Cells were grown in LB medium supplemented with 25 µM IPTG.

Figure S22
Brunet et al.

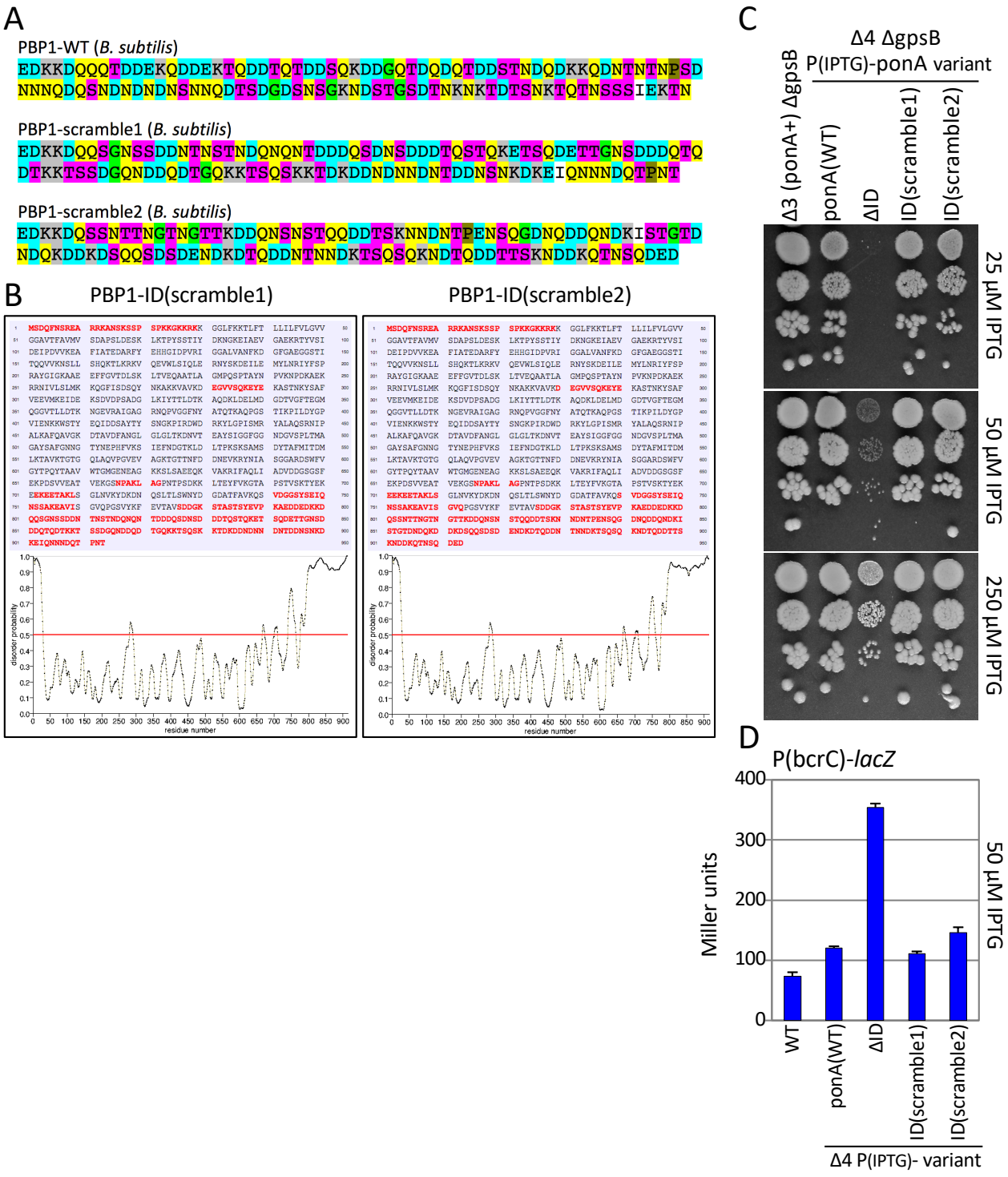

Figure S22. An intrinsically disordered region on PBP1 is important for function. **(A)** Amino acid sequences of the the native IDR of PBP1 and two variants in which the order of the amino acids were scrambled. Residues with similar properties are colored identically. **(B)** Both scrambled IDRs are predicted to be intrinsically disordered. Graphical output from PrDOS (Ishida & Kinoshita, 2007). **(C)** Spot dilutions of the indicated strains on LB agar plates supplemented with IPTG. Both scrambled IDRs function similarly to wild-type. **(D)** Bar graph showing β-galactosidase activity from a σ^{I}-responsive reporter in the indicated strains grown in LB with 50 μM IPTG. Error bars represent standard deviation from three biological replicates.

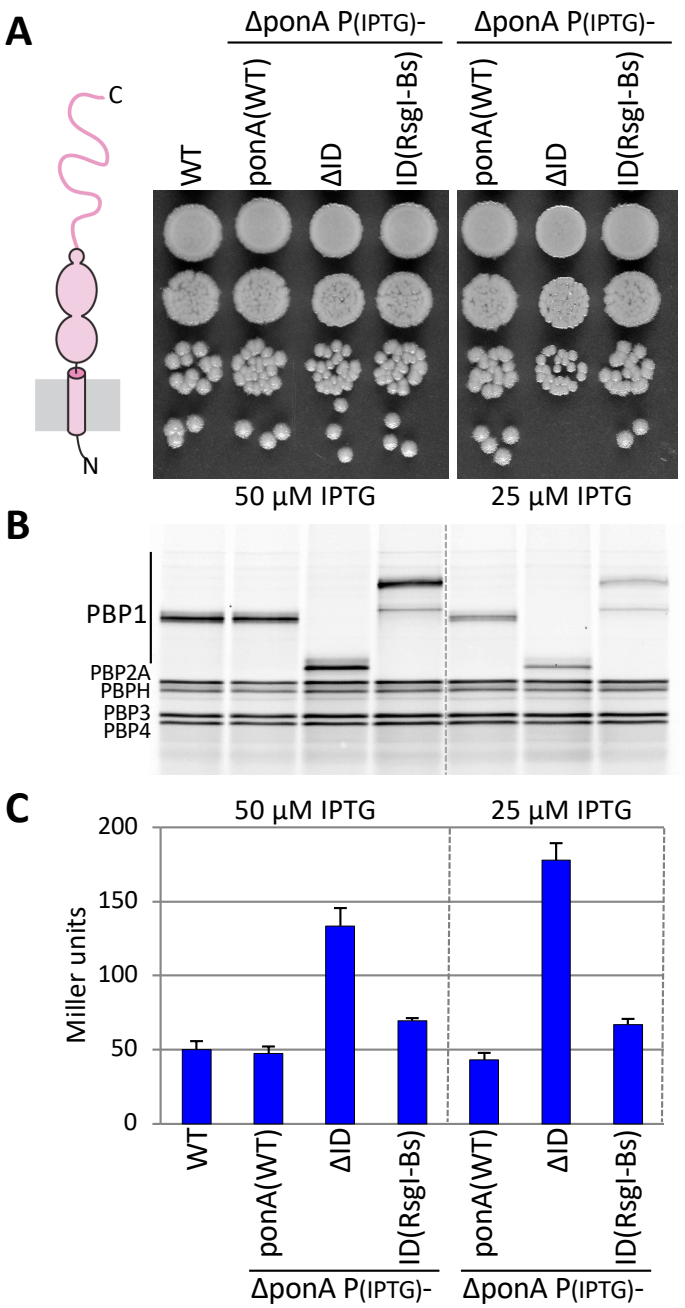

Figure S23. Cell expressing PBP1 without its intrinsically disordered region induce σ^{I} even under conditions where growth is not impaired. (A) Spot dilutions of the indicated strains on LB agar plates supplemented with IPTG. All strains contain native *pbp4*, *pbpF*, and *pbpG*. The only gene deletion is *ponA*. **(B)** Bocillin gel of the same strains shown in A. **(C)** Bar graph showing β-galactosidase activity from the σ^{I}-responsive reporter P(bcrC)-*lacZ* in the indicated strains grown in LB with 25 or 50 µM IPTG. Error bars represent standard deviation from three biological replicates.